The Role of Aquaporin-4 in Subarachnoid Haemorrhage

Thesis submitted for the degree of Doctor of Medicine

Matthew Tait

Exeter College

Michaelmas 2011

Abstract

Introduction. The glial cell water channel aquaporin-4 (AQP4) plays an important role in brain oedema, astrocyte migration and neuronal excitability. Current theories of AQP4 function are based largely on experiments using AQP4 -/- mice. These mice have only been partially characterized. I therefore undertook a detailed investigation of baseline brain properties in AQP4 -/- mice. In the second part of my experiments I investigated the role of AQP4 in brain oedema in a mouse model of subarachnoid haemorrhage.

Method. Gross anatomical measurements included estimates of brain and ventricle size. Neurons, astrocytes and oligodendrocytes were assessed using the neuronal nuclear marker NeuN, the astrocyte marker GFAP, and the myelin stain Luxol Fast Blue. The blood brain barrier was studied by electron microscopy and the horseradish peroxidase extravasation technique.

A mouse model in which 30µl of autologous blood was injected into the basal cisterns was used to reproduce subarachnoid haemorrhage. Brain water content, intracranial pressure and neurological score were compared in wildtype and AQP4 -/- mice. I also measured blood brain barrier permeability and the osmotic permeability of the glia limitans, one of the routes of oedema elimination.

Results. There were no differences in brain and ventricle sizes between wildtype and AQP4 -/- mice, nor were there differences in the cerebral cortical density of NeuN

positive nuclei, perimicrovessel and glia limitans GFAP immunoreactivity, or the thickness and myelination of the corpus callosum. The ultrastructure of microvessels in the frontal cortex and caudate nucleus of wildtype vs. AQP4 -/- mice was indistinguishable, with features including intact endothelial tight junctions, absence of perimicrovessel astrocyte foot process oedema, and the absence of horseradish peroxidase extravasation.

Wildtype and AQP4 -/- mice had comparable baseline brain water content, intracranial pressure and neurological score. At 6hr after blood injection, AQP4 -/- mice developed more brain swelling than wildtype mice. Brain water content increased by 1.5 +/- 0.1% vs. 0.5 +/- 0.2% (mean +/- standard error, $P<0.0005$) and intracranial pressure by 36 +/- 5 vs. 21 +/- 3mmHg ($P<0.05$) above pre-injection baseline, and neurological score was worse at 18.0 vs 24.5 (median, $P<0.05$), respectively. Although subarachnoid haemorrhage produced comparable increases in blood barrier permeability in wildtype and AQP4 -/- mice, AQP4 -/- mice had a twofold reduction in glia limitans osmotic permeability.

Conclusions. My data show that AQP4 deletion in mice does not produce major structural abnormalities in the brain. The AQP4 -/- mouse is therefore a reliable subject for experiments in cerebral oedema. My investigation of cerebral oedema in subarachnoid haemorrhage showed that AQP4 -/- mice manifest increased brain oedema following subarachnoid haemorrhage. This is due to reduced elimination of excess brain water.

Presentations

1. Aquaporin-4 Deletion in Mice Increases Brain Oedema after Subarachnoid Haemorrhage. MJ Tait, BA Bell, MC Papadopoulos. XIV International Symposium on Brain Oedema and Brain Tissue Injury, Warsaw, Poland 12th June 2008

2. Aquaporin 4 and subarachnoid haemorrhage. MJ Tait, BA Bell, MC Papadopoulos. British Neurosurgical Research Group, London February 14-15th 2008

Papers

1. Water movements in the brain: role of aquaporins. MJ Tait, S Saadoun, BA Bell, MC Papadopoulos. *Trends Neurosci*. 2008 Jan;31(1):37-43

2. AQP4 gene deletion in mice does not alter blood-brain barrier integrity or brain morphology. S Saadoun, MJ Tait, A Reza, DC Davies, BA Bell, AS Verkman, MC Papadopoulos. *Neuroscience.* 2009 Jul 7;161(3):764-72.

3. Increased brain oedema after subarachnoid hemorrhage in *aqp4*-null mice. MJ Tait**,** S Saadoun, AS Verkman, BA Bell, MC Papadopoulos. *Neuroscience.* 2010 Apr 28;167(1):60-7.

Table of Contents

Table of Figures

Introduction

Brain oedema is a devastating condition associated with many brain pathologies. In this study I investigated the role of the water channel aquaporin-4 in brain swelling produced by a common neurosurgical condition, spontaneous subarachnoid haemorrhage.

1.0 Brain water homeostasis.

Brain oedema occurs due to a disruption of the normal brain water homeostasis. I will begin with a description of water flow in the brain under normal physiological conditions.

The normal adult human intracranial cavity (~1.4 L) consists of four major physiological compartments: blood (50-100 mL), cerebrospinal fluid (CSF) (100-150 mL), brain intracellular (0.9-1.2 L) and extracellular (100-150 mL) spaces (ICS and ECS)(Crockard et al. 2000). Under normal conditions, water flows between these compartments in response to osmotic and hydrostatic forces producing a dynamic system of interrelated fluid spaces.

1.0.1 Intracranial supply of water

Water enters the brain from the arterial compartment via one of two routes. The principle route of entry is via the brain capillary bed directly into the brain parenchyma. This takes place at approximately 0.17µl/g/min (Crockard et al. 2000). In contrast to other capillary beds, the vascular endothelium within the CNS limits trans-capillary flow. This reduced capillary permeability is referred to as the blood

brain barrier (BBB) and is produced by both specially adapted capillary endothelial cells and the foot processes of adjacent astrocytes. Unlike capillary beds outside the central nervous system, brain endothelial cells are linked by tight junctions, lack fenestrations and have few endocytotic vesicles (Reese and Karnovsky 1967; Sage et al. 1998).

Astrocytes are a subset of glial cells that are found in close proximity to the brain capillaries forming an intrinsic part of the BBB. Each capillary is tightly encircled by astrocyte foot processes. This close proximity of astrocyte foot processes to the endothelium means that fluid crossing the capillary wall does not pass into the general extracellular space but into the intracellular space of the adjacent astrocytes. This gives a further potential site at which flow across the BBB can be controlled. Fluid may then enter the extracellular space across the astrocyte plasma membrane. The altered endothelium and surrounding astrocyte foot processes act as a functional unit to form the BBB. Furthermore, astrocytes produce factors that induce the formation of the BBB capillary adaptations (Janzer and Raff 1987).

The presence of a BBB has several consequences. Most importantly it allows greater control over the passage of water and solutes into and out of the brain. There is, therefore, close regulation of brain volume and protection from blood borne toxins. An intact BBB disrupts the normal balance of Starling's capillary forces: the tight junctions reduce the impact of hydrostatic forces so that osmotic pressure is the dominant force driving water out of the capillary. This also reduces the effectiveness of the capillary bed in removing fluid from the brain parenchyma.

1.0.2 The extracellular space

Approximately 20% of the total brain volume is extracellular space (Sykova 1997). It contains a jelly-like extracellular matrix that forms the microenvironment for cells and is therefore vital to their function (Sykova 1997). The extracellular fluid delivers and removes metabolic substrates and waste including gases; it provides extracellular ions both to supply the intracellular compartment and to generate membrane potentials and it is the medium for non-synaptic intercellular messaging (Fields and Stevens-Graham 2002). The low protein content of extracellular fluid is thought to benefit the electrical function of cells. The BBB helps maintain a constant extracellular fluid composition.

Maintenance of extracellular fluid volume is vital to all of these functions. Molecules move through the extracellular space by diffusion (Nicholson et al. 2000). The rate of diffusion is altered by both the local volume and tortuosity of the extracellular space (Nicholson et al. 2000; Sykova and Nicholson 2008). Tortuosity is a measure of the impact of the highly complex shape of the extracellular space on diffusion. Changes in either the volume or shape of the extracellular space will therefore alter the rate of molecular diffusion and result in deterioration of the cellular microenvironment.

1.0.3 The intracellular space

Once in the extracellular space, water is exchanged across the plasma membranes of neurons and glial cells to form the intracellular fluid. Regulation of this flow is according to the ionic, metabolic and volumetric homeostasis of individual cells.

1.0.4 The CSF space

Cerebrospinal fluid (CSF) is distributed between the ventricular system (25%) and the cisterns of the cranial and spinal subarachnoid spaces (Kohn et al. 1991). It provides a cushion for the brain and spinal cord as well as allowing removal of metabolites, toxins and neurotransmitters (P. D. Brown et al. 2004).

Production of CSF constitutes the second major way that water enters the intracranial system. The CSF formation rate is approximately 20 ml/hour or 500ml/day (Cutler et al. 1968; Milhorat et al. 1971). It is mainly produced by the choroid plexus within the ventricles. This takes place by ultrafiltration of plasma across the endothelial capillary wall and by active transport of sodium and bicarbonate by the choroidal epithelium (P. D. Brown et al. 2004). Additionally, 10-30% of CSF is produced by drainage of extracellular fluid from the brain (Milhorat et al. 1971).

1.0.5 Drainage of intracranial water

Fluid either leaves the extracellular space by bulk flow into the CSF or back into the capillaries via Virchow's spaces. Passage into the CSF is either via the pia mater (into the CSF cisterns) or across the ependyma (into the ventricles). In order to exit via either surface water must cross the glia limitans, which is a specialized layer of astrocytes that forms the outermost layer of neural tissue. It is divided into two areas: glia limitans interna or externa. The glia limitans externa faces the subarachnoid CSF spaces. It consists of a dense sheet of astrocytes and their foot processes. The foot processes adhere to a basement membrane, which is in turn connected to the pia mater (Owens et al. 2008). Glia limitans externa astrocytes are not connected by tight

junctions but the high cell density of the layer does act as a barrier to water passage. The glia limitans interna faces the ventricular CSF space. The astrocyte cell layer here is not as thick and, together with the ependyma forms a leaky barrier between CSF and extracellular fluid (Del Bigio 1995)

Water is ultimately reabsorbed from the CSF into the venous system via the arachnoid granulations. These out-pouchings of arachnoid through the dura into the dural venous sinuses bring the CSF into close proximity with the blood. Water crosses the arachnoid via giant vacuoles that span the arachnoid cells (Tripathi and Tripathi 1974). Ultrastructural studies do not support the idea that arachnoid granulations contain valves (Tripathi and Tripathi 1974). Increased ICP leads to increased formation of vacuoles reflecting an increased absorption rate in response to demand (Davison and Segal 1996).

A further difference between water circulation in the brain and rest of the body is the absence of lymphatics in the central nervous system. Although controversial, evidence does exist for a connection between the CSF and the extracranial lymph system: tracers injected into human cadaver brain are found in the cervical and spinal lymph nodes (Foldi 1999) and malignant gliomas preferentially metastasize to the cervical lymph nodes and lung (Hoffman and Duffner 1985). The likely anatomical sites are the cribriform plate, where the olfactory nerve perineural space may communicate with nasal submucosa lymphatics, and the spine although the exact spinal location is contested (Koh et al. 2005). Spinal lymphatic absorption of CSF

may be considerable: 6.6 to 13.8 mL/hour has been measured in humans (Edsbagge et al. 2004).

1.1 Definition of brain oedema

Brain oedema is an increase in the total fluid within the brain parenchyma, associated with an increase in total brain volume (Fishman 1975). It is formed in response to a pathological alteration of either the membranes separating the fluid spaces or the osmotic or hydrostatic gradients across them. The excess fluid alters the relative volumes of the different fluid compartments within the brain.

Oedema has both formation and resolution phases. Oedema forms when water enters the brain (formation) faster than it can be drained (resolution). This may occur due to a pathological increase in the rate of formation of intraparenchymal brain water or because of a decrease in the rate of elimination as the primary event. Different forms of cerebral oedema are recognised. Cytotoxic oedema and vasogenic oedema are the result of increased formation. Interstitial oedema is primarily because of reduced elimination.

Once the oedema has been established it is maintained by a balance in the formation and elimination of excess fluid. Resolution can only take place when water drains from the brain faster than it enters.

1.2 Formation of brain oedema

Four main types of brain oedema have been described; vasogenic, cytotoxic, interstitial and osmotic. In both vasogenic oedema and interstitial oedema there is abnormal fluid collection in the extracellular space whereas cytotoxic oedema and osmotic oedema both cause an increase in intracellular volume. Each has a different mechanism of formation (Klatzo 1994). I will consider each separately.

1.2.1 Formation of vasogenic oedema

Vasogenic oedema occurs when the BBB integrity fails. The BBB prevents over accumulation of fluid within the brain extracellular space by negating the effect of capillary hydrostatic pressure and limiting the passage of osmotically active molecules. When the BBB fails, hydrostatic forces cause extravasation of a protein-rich exudate from plasma, through the leaky BBB into the extracellular space resulting in cerebral oedema (Klatzo 1994; Kuroiwa et al. 1985; Reulen et al. 1977) **(Figure 1A)**.

Vasogenic oedema is seen in brain tumours (Seitz and Wechsler 1987), brain abscesses (Lo et al. 1994), haemorrhage, seizures, radiation injury and hypertensive encephalopathy (Nag et al. 2009b). The rate of formation may be very rapid but varies by source. For example, CT scan analysis shows oedema propagation rates of 0.09-1.63 ml/hr in cerebral metastases and 0.42-3.39 ml/h in gliomas (Groger et al. 1994). The increase in extracellular fluid occurs predominantly in the white matter probably because water flow in the white matter extracellular space is along

streamlined nerve fibres and so is easier than flow within the extracellular space of gray matter which is a complex mesh of cell fibres (Nag et al. 2009b).

The pathophysiology of BBB breakdown in vasogenic oedema involves reversal of the adaptations of BBB endothelium. Study of the BBB ultrastructure in the early stages of vasogenic oedema shows fenestrations and increased endocytotic activity (Nag 2003). This is associated with increased expression and phosphorylation of Cav-1, an integral membrane protein involved in transport of proteins across the endothelium (Nag et al. 2007; Nag et al. 2009a). Breakdown of the tight junctions occurs later in the course of oedema formation (Brightman et al. 1983). Reduced expression of the tight junction proteins JAM-A, claudin-5 and occludin is seen between 0.5 and 6 days after BBB breakdown (Nag et al. 2007; Yeung et al. 2008). Histamine, bradykinin, leukotriene C4 and vascular endothelial growth factor-A have all been shown to induce BBB breakdown under experimental conditions (Dobrogowska et al. 1998; Nag 2003).

1.2.2 Formation of cytotoxic oedema

The second major type of brain oedema is cytotoxic oedema, caused by cell swelling and is thus associated with a reduced extracellular volume and an intact BBB (Klatzo 1987). Loss of fluid from the extracellular space causes extracellular osmolality to rise and water crosses the intact BBB due to an alteration in osmotic forces caused by cellular dysfunction **(Figure 1B)**. Cerebral ischaemia (Ayata and Ropper 2002), traumatic brain injury (Unterberg et al. 2004), and metabolic disorders such as hepatic or renal failure (Vaquero and Butterworth 2007) all cause cytotoxic oedema.

In cytotoxic oedema the primary insult generally occurs outside the brain leading to an alteration in the composition of the extracellular fluid resulting in a change in the cells' micro-environment. Vasogenic oedema, by contrast, is often the result of disease processes that take place within the brain. Cytotoxic oedema has been studied most intensively in cerebral ischaemia. Failure to supply metabolites and oxygen causes cells to become 'sick'. Na^+/K^+ ATPase channels in the plasma membrane have a high energy requirement and once these fail the $[Na]_i$ rises and water enters the cell down an osmotic gradient (Fishman 1975; Ito et al. 1979; Schoonman et al. 2008). The resulting rise in extracellular osmolality causes water to enter the brain via the BBB resulting in swelling.

Cytotoxic oedema is not spread evenly throughout the affected cells. All brain cell types swell but not equally: swelling primarily takes place in astrocytes rather than neurons, dendrites or endothelial cells. This may be because of the high permeability to water of astrocytes due to the presence of AQP4 water channels or because their role in K^+ and glutamate clearance predisposes them to high intracellular osmolality. Astrocytes are 20x more common than neurons in human brain and are able to swell to five times their normal size making astrocyte swelling the dominant ultrastructural finding of cytotoxic oedema (Kimelberg 1995).

In the initial stages of cytotoxic oedema swelling is not uniform within the astrocyte either. Early cytotoxic oedema is predominantly found in the astrocyte foot processes (Wasterlain and Torack 1968). This may be due to the proximity of the foot

processes to the BBB. The foot process is highly permeable to water even when compared to the rest of the rest of the astrocyte membrane (due to a high density of AQP4 water channels – see below 3.2). If the rate of water flow across the BBB and through the astrocyte is abnormally high then water may ‘back up’ in the foot process causing swelling. Alternatively foot process swelling may be due to an attempt by the cell to stop water entering the extracellular space.

Cytotoxic oedema results in reduced ECF volume and increased tortuosity leading to reduced diffusion. Dead space microdomains also form in which no diffusion takes place (Binder et al. 2004). This further hinders the ability of the extracellular space to support the cells resulting in further cellular injury and swelling. Additionally, the reduced extracellular space results in decreased ability to clear oedema fluid. By contrast, vasogenic oedema results in increased extracellular volume.

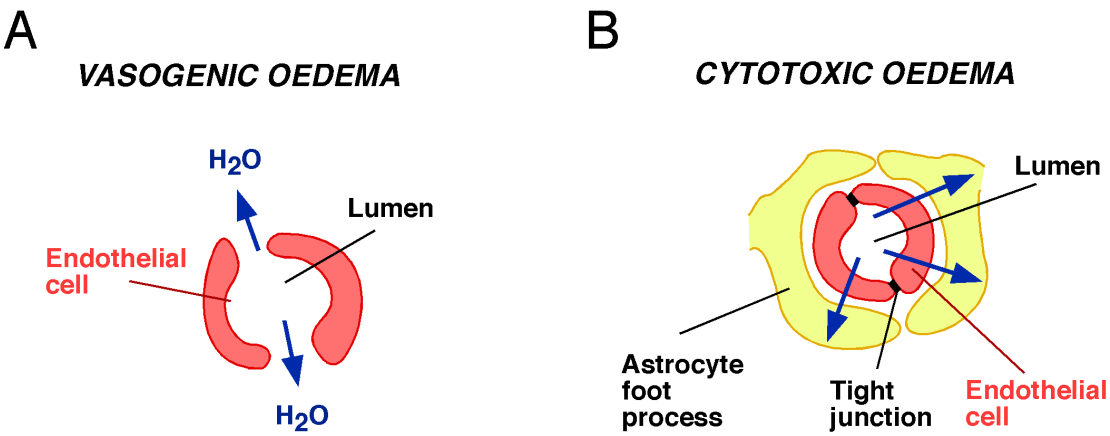

Figure 1. Formation of cerebral oedema. **A.** In vasogenic oedema, water moves from blood down a hydrostatic pressure gradient through a leaky BBB into the brain ECS. **B.** In cytotoxic oedema, water moves from the blood through endothelial cells and astrocyte foot process membrane into the brain. [Adapted from Tait MJ *et al.* Water movements in the brain: role of aquaporins. *Trends Neurosci*. 2008 Jan;31(1):37-43.]

1.2.3 Interstitial oedema

Interstitial oedema is also called hydrocephalic oedema. Like vasogenic oedema it results in an increase in the extracellular fluid volume but unlike vasogenic oedema it is caused by insufficient drainage of *normal* extracellular fluid rather than over production of *abnormal* extracellular fluid. This results in an expanded extracellular space but a normal intracellular volume.

Interstitial oedema is best characterized in hydrocephalus. A blockage in CSF flow or drainage causes the CSF pressure to rise. Although most CSF is produced by the choroid plexus, up to 30% is from trans-ependymal drainage of extracellular fluid (Milhorat et al. 1971). When CSF pressure is high this drainage does not take place resulting in interstitial brain oedema due to increased extracellular fluid (Fishman 1975). Other causes of decreased brain water clearance are less well studied, for example, venous sinus occlusion would be expected to produce interstitial oedema.

The impact of hydrocephalic interstitial oedema *per se* on brain function is unclear as patients also have raised CSF pressure and therefore raised intracranial pressure. The excess fluid is evident on CT and MR scans as 'periventricular lucencies'. The principle clinical implication of hydrocephalic oedema is as a radiological sign indicating rising CSF pressure in those with ventriculomegaly. Resolution of hydrocephalic oedema will only take place once CSF flow has been restored.

1.2.4 Osmotic oedema

In common with cytotoxic oedema, osmotic oedema is the result of an extracranial

process and results in intracellular oedema (Gullans and Verbalis 1993). In both cases the extracellular milieu is unable to support normal cell function. Osmotic oedema may be the result of inappropriate antidiuretic hormone secretion, diabetic ketoacidosis or excessive haemodialysis (Doczi et al. 1982). A fall in plasma osmolality results in an osmotic gradient from the intracellular compartment to the plasma with a rise in intracellular volume as water flows into the cells. The BBB remains intact. In contrast to cytotoxic oedema there is not metabolic disturbance to the swollen cells.

1.3 Resolution of cerebral oedema

For resolution to take place elimination of excess fluid must occur faster than production. Resolution therefore requires both drainage of excess fluid and reduction of oedema production (as mechanisms of fluid drainage must have been overwhelmed in order to produce oedema in the first place).

Resolution of vasogenic oedema begins as soon as impermeability of the BBB to proteins is restored. Elimination of excess fluid was originally thought to be by bulk flow rather than diffusion. Excess fluid is cleared into subarachnoid CSF (Ohata et al. 1990), ventricular CSF (Reulen et al. 1977) and also drained via the perivascular spaces (Cserr et al. 1981) **(Figure 2)**. Approximately 90% of clearance is into the CSF (Marmarou et al. 1994). Oedema fluid passes down hydrostatic pressure gradients into the CSF where it is eventually returned to the blood via the arachnoid granulations (Reulen et al. 1977; Reulen et al. 1978; Tsuyumu et al. 1981).

In order to drain into the CSF water must cross the glia limitans. The bulk flow theory would require water to pass between cells in this densely cellular area. The acceptance of bulk flow is based on experiments that use radiolabelled dyes to track flow of extracellular fluid (Reulen et al. 1978; Tsuyumu et al. 1981). These experiments do not allow for the possibility of a route of water egress that is specific to water. As a result they assume that the marker is eliminated through the same route as the water, which would not be true if water is eliminated via an AQP mediated pathway. The high density of AQP4 channels at the glia limitans strongly suggests that water is able to pass through the cells by diffusion rather than around them by bulk flow. This pathway would not be detectable by any techniques involving dyes or markers as these are unable to pass through AQP4. This diffusion pathway has yet to be demonstrated experimentally.

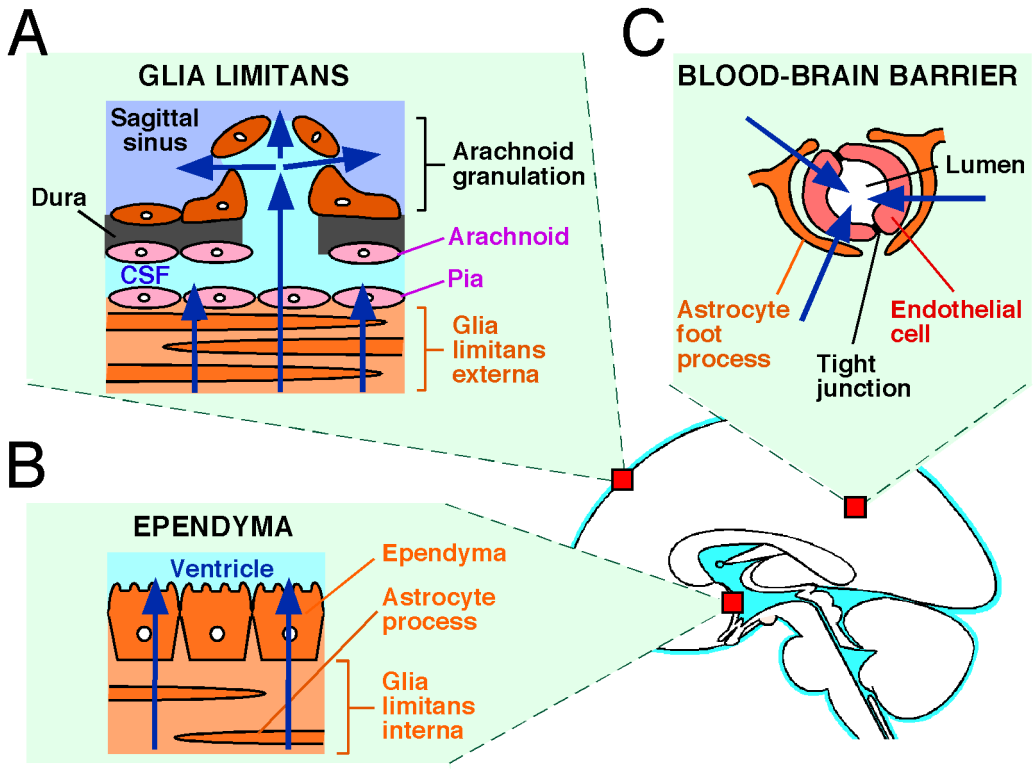

Figure 2. Resolution of cerebral oedema. A. Excess water moves from brain, through several layers of astrocyte processes comprising the glia limitans externa and pia into subarachnoid CSF. B. Excess water also moves from brain, through layers of subependymal astrocyte processes (glia limitans interna) and ependyma into ventricular CSF. C. Some excess water moves from brain through astrocyte foot processes and endothelial cells into the blood. [Adapted from Tait MJ *et al.* Water movements in the brain: role of aquaporins. *Trends Neurosci*. 2008 Jan;31(1):37-43.]

1.4 Consequences of cerebral oedema

Oedema may occur in any organ but for the brain it presents a unique set of problems. As the brain swells it is limited by the non-compliant skull. Initially other intracranial contents particularly venous blood and CSF are expelled from within the skull preventing a rise in the intracranial pressure (ICP). Both venous blood and CSF are highly viscous and are contained in compressible spaces that communicate easily with the extracranial space. Venous blood is contained in both veins and dural sinuses that communicate with the rest of the venous system via the jugular foramen and CSF within the ventricular system communicates freely with the spinal cisterns. Displacement of liquid volume allows the intracranial pressure to remain stable initially as the brain volume increases. Once all the available CSF and venous blood have been extruded, further brain swelling causes a rise in ICP. This exponential volume-pressure relationship is referred to as the Monro-Kellie doctrine. If brain volume rises very slowly (e.g. due to slow growing mass lesion) then extracellular fluid can also be expelled from the intracranial vault resulting in sometimes remarkable changes in the volume of the brain parenchyma. Critically raised ICP results in brain ischaemia, herniation and, eventually, coma and death.

1.5 Treatment of cerebral oedema

Focal vasogenic oedema such as that caused by brain tumours can be treated with glucocorticoids such as dexamethasone. Current treatments for global cerebral oedema are complex and have limited efficacy. There has been little change in the mainstays of treatment in last 50 years (Matson 1965). Three broad approaches are taken; (1) reduction of fluid within the brain parenchyma by altering the osmotic

gradient between plasma and brain ECS using hyperosmotic agents such as hypertonic saline or mannitol; (2) prevention of cerebral ischaemia by optimizing arterial supply, reducing metabolic demand by inducing coma or maximizing venous drainage of the brain and (3) surgical measures such as external ventricular drainage or decompressive craniectomy (Reviewed in (Rabinstein 2006)).

2.1. General aspects of Aquaporins.

Aquaporins (AQPs) are a family of water channel proteins, which increase plasma membrane osmotic permeability. Experiments long before the discovery of AQPs showed that red blood cell membranes are more permeable to water than would be expected from water diffusion through the hydrophobic lipid bilayer alone. This led to a strong suspicion of the existence of another means by which water could cross the plasma membrane (Sidel and Solomon 1957). In 1988 Peter Agre discovered the first water channel, termed AQP1 (Denker et al. 1988), and was awarded the Nobel Prize in Chemistry in 2003. He subsequently showed that frog oocytes expressing AQP1 in their plasma membrane were far more susceptible to osmotic lysis than non-expressing oocytes (Preston et al. 1992), thus proving that AQP1 transports water. To date, at least 13 AQPs have been found in mammals and more than 300 in lower organisms.

AQPs selectively pass water, except for a sub-group, known as aquaglyceroporins (AQP3, AQP7, AQP9), which also pass glycerol and some small non-polar molecules.

Most of our knowledge of the roles of AQPs in different tissues comes from experiments with AQP -/- mice (reviewed in (Verkman 2005)). In general, AQPs increase water permeability across epithelia allowing fast water flow to accompany active salt transport. This principle is illustrated by AQP5 deletion in mice, which causes the salivary and airway submucosal glands to secrete a low volume of relatively hypertonic fluid (Song and Verkman 2001; Song et al. 2002). AQPs also

facilitate water flow in response to passive osmotic gradients. For example, AQPs increase osmotic re-absorption of water from renal collecting ducts and, as a result, AQP deficient mice (AQPs 2 – 4) have impaired ability to concentrate urine (Verkman 2006).

Several aquaglyceroporin functions have been described, related to their glycerol transporting ability. In humans and rodents, AQP3 is found in skin keratinocytes. AQP3 -/- mice have a dry, scaly skin because of reduced glycerol content in the stratum corneum and epidermis (Hara et al. 2002; Hara and Verkman 2003). AQP7 is expressed in fat cells and mice lacking AQP7 carry more fat than wildtype mice (Hara-Chikuma et al. 2005). Because cell membrane glycerol permeability of AQP7 deficient fat cells is reduced, glycerol accumulates within the cell and stimulates triglyceride synthesis.

2.2. Aquaporins and CNS function.

Three aquaporins have been identified within the CNS: AQP1, AQP4 and AQP9. By far the most prominent and most studied is AQP4, which appears to play a major role in brain oedema pathophysiology. I will briefly consider the other two first.

2.2.1. Aquaporin-1. AQP1 is expressed in the apical membrane of the choroid plexus, and plays a role in forming CSF (Oshio et al. 2005). AQP1 is upregulated in choroid plexus tumours (Longatti et al. 2006), which are associated with increased CSF production, again supporting a role for AQP1 in CSF secretion. Interestingly, AQP1 is not found in normal brain capillary endothelium, although highly expressed

in peripheral endothelial cells (Dolman et al. 2005; Nielsen et al. 1993). Cerebral capillary endothelial cells cultured in the absence of astrocytes (Dolman et al. 2005), and capillary endothelial cells within brain tumours (which are not surrounded by astrocyte endfeet) express AQP1 (Saadoun et al. 2002b). These observations suggest that astrocyte endfeet may signal adjacent endothelial cells to switch off endothelial AQP1 expression, although the precise signaling remains unknown. AQP1 is also found in small diameter sensory neurons in dorsal root, trigeminal, and nodose ganglia, but studies of a possible role for AQP1 in pain sensation have yielded conflicting results (Oshio et al. 2006; Shields et al. 2007).

2.2.2. Aquaporin-9. AQP9 immunoreactivity in rat brain has been observed in some white matter astrocytes, Bergmann glia, and a subpopulation of glia called tanycytes (Reviewed in (Badaut and Regli 2004)). Since AQP9 transports energy substrates (glycerol, lactate), AQP9 may play a role in controlling cerebral energy metabolism. Further support for this idea comes from reports of AQP9 immunoreactivity in glucose-sensitive catecholaminergic neurons (Badaut and Regli 2004) and in mitochondria (Amiry-Moghaddam et al. 2005). In general, AQP9 protein expression becomes upregulated in several brain diseases (Reviewed in (Badaut and Regli 2004)) including astrocytes bordering cerebral infarcts in mice. It has been suggested that AQP9 facilitates the clearance of lactate during reperfusion. Caution is required when interpreting AQP9 protein expression studies though: the comparable AQP9 immunoreactivities seen in the brains of wildtype and AQP9 -/- mice (Rojek et al. 2007) suggest that AQP9 antibodies might cross-react with other proteins giving false positive data for AQP9 expression.

2.2.3 Aquaporin-4 AQP4 is the principal AQP in mammalian brain (Badaut et al. 2002). Experiments to date have implicated AQP4 in three main areas; CNS water homeostasis; astrocyte migration and regulation of neuronal activity. Before considering the role of AQP4 in each of these I will describe the properties of the AQP4 channel itself.

3.1 AQP4 - Structure

In order to understand the function of AQPs it is necessary to understand their structure. Most detailed work on AQP structure has been performed on AQP1 but AQP4 is structurally very similar. Even so, important differences are found which will be discussed.

3.1.1 Structure of AQPs in general

The AQPs are proteins that assemble in cell membranes as tetramers (Agre et al. 2002; Verkman 2005). Each monomer is about 30 kDa and has six transmembrane domains surrounding a water channel **(Figure 3A)** (Shi et al. 1994). Thus each AQP molecule contains four water pores although the advantage of this unusual structure is unknown (Neely et al. 1999). Each transmembrane domain is an α-helix. The helices are arranged in a ring around the central pore each at a right handed 30° tilt leading to an hourglass shaped central channel with a tight central constriction (Cheng et al. 1997; Sui et al. 2001; Walz et al. 1997). The six α-helices are separated by 5 loops (A-E). Loops B and E both contain a highly conserved NPA (asparagine, proline, alanine) sequence and a short helix (Preston et al. 1992) **(Figure 3B)**

The inside of the central channel is predominantly hydrophobic with two narrowings. At the midpoint of the channel the highly conserved NPA motifs form a pore less than 3Å wide. Towards the extracellular vestibule of the channel is a second constriction: the Ar/R (aromatic/ arginine) constriction. The Ar/R pore is the narrowest point of the channel at 2Å (Sui et al. 2001). Individual water molecules are approximately 2Å wide at their longest axis so water molecules must pass through the pore in single file. As water is the smallest organically active molecule this narrow constriction acts as a physical barrier to other molecules.

Protons exist in solution as hydronium ions (H_30^+). This molecule is unstable and the additional H^+ can transfer to adjacent water molecules (called the Grotthuss mechanism). Molecular dynamics studies have shown that the point of highest resistance to water passage is the NPA site (Murata et al. 2000) where a strong electrostatic field spans the pore (de Groot et al. 2003). This field is generated mainly by the helical macrodipoles of the B and E loops and is proposed to be the cause of proton specificity.

The molecular structure of the channel also accounts for its high permeability to water compared to the plasma membrane. Resistance is reduced by bypassing the hydrophobic middle portion of the plasma membrane. The main resistance involved in passage through an aquaporin channel is the disruption of the intermolecular van der Waal's forces required to align water molecules in single file. The energy required to do this is reduced by the arrangement of ionic charges within the channel.

3.1.2 Structure of AQP4

The structure of the AQP4 channel means that water can pass in either direction at the same rate (Meinild et al. 1998). Furthermore, the channel seems always to be open: phosphorylation of AQP4 does not alter function (Yang and Verkman 1997). AQP4 has a particularly high permeability to water even when compared to other AQPs (Yang et al. 1997; Yang and Verkman 1997). Artificial induction of AQP4 expression in Xenopus oocytes results in an approximately 40-fold increase in water permeability (Yang and Verkman 1997). Single channel permeability of AQP4 to water is 24 +/- 0.6 x $10^{-14}cm^3/s$ (the next most permeable channel measured in this study was AQP1 at 6 x $10^{-14}cm^3/s$) (Yang and Verkman 1997). The basis for the particularly high permeability of AQP4 to water is likely to be molecular but remains unknown.

Two isoforms of AQP4 have been discovered: M1 and M23. The two isoforms differ at the N terminus: translation of the AQP4 gene may be initiated at the first methionine (M1) or the second methionine (M23) (Lu et al. 1996) (Jung et al. 1994) (Neely et al. 1999). M23 is approximately three times more abundant than M1. No functional difference in the water permeabilities of M1 and M23 have been identified (Jung et al. 1994) (Neely et al. 1999) but the ratio of the two isoforms is important to the pattern of expression of AQP4 on the plasma membrane.

AQP4 molecules form unique, highly regular grids of proteins known as orthogonal arrays of particles (OAPs). These are visible on the plasma membrane using freeze fracture electron microscopy. Transfection of rat AQP4 cDNA into Chinese hamster

ovary (CHO) cells results in the appearance of OAPs (Ma et al. 1996). CHOs with just M23s have large regular OAPs, many containing 10x more AQP4 tetramers than OAPs seen in the brain. By contrast the CHOs with only M1 polypeptides produced a disorganized pattern of expression with many individual tetramers or very basic square lattices. CHOs with both M1 and M23 showed OAPs with a range of sizes, more in keeping with those seen in nature. M1 and M23 can heterotetramise in any ratio but only M23 can bind to adjacent tetramers to form OAPs (Tajima et al. 2010). It is therefore likely that the cell is able to maintain the optimum size of OAPs by adjusting the ratio of M1 and M23 as increasing the M23:M1 ratio increases the size of the arrays (Furman et al. 2003; Tajima et al. 2010).

Although the advantage of OAP formation is unknown, AQP4 function in both brain water homeostasis and cell motility does depend on the induction of high degrees of water permeability at specific places on the cell membrane. The OAPs allow a very high density of channels in a specific region. This is termed polarity and is considered in detail below. OAPs are known to break down under certain pathological conditions so the size of the OAPs seen in the brain may reflect a pay off between the advantage gained from OAPs and the speed with which they can be dissembled (Furman et al. 2003). Furthermore, it is likely that large lattices of channels will alter the stiffness of the membrane perhaps hindering cell function such as the ability of the cell membrane to deform during migration through tight spaces.

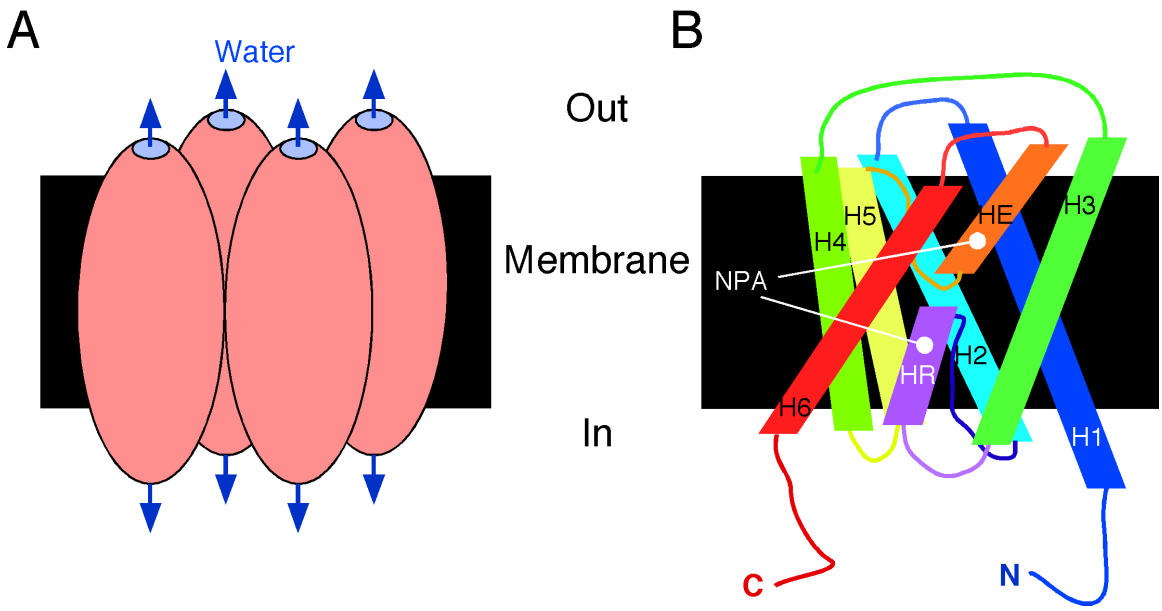

Figure 3. Schematic showing AQP1 structure. A. Tetrameric arrangement of AQP1 in membrane. Each monomer has a water pore. **B.** AQP1 monomer consists of 6 alpha-helical domains (H1 - H6) around a water pore, 2 conserved NPA motifs (Asn-Pro-Ala) that allow water but not small solutes to pass across the pore, and intracellular N- and C-termini. [Adapted from Tait MJ *et al.* Water movements in the brain: role of aquaporins. *Trends Neurosci*. 2008 Jan;31(1):37-43.]

3.2. AQP4 - sites of expression

AQP4 was first cloned from rat lung (Hasegawa et al. 1994) and has been found in electrically excitable tissues including brain, spinal cord, retina, inner ear, and skeletal muscle (Hasegawa et al. 1994; J. Li and Verkman 2001; J. Li et al. 2002; Nielsen et al. 1997; Oshio et al. 2004; Rash et al. 1998; Yang et al. 2000). A general principle is that AQP4 is not expressed in excitable cells, but is found in supporting cells (astrocytes and ependyma in the CNS; Müller glia in the retina; Hensen's, Claudius, and inner sulcus cells in the ear).

Brain AQP4 is strongly expressed at the borders between the brain parenchyma and the adjacent major fluid compartments. At the BBB the adjacent astrocytes express AQP4 strongly. AQP4 in these astrocytes is not evenly expressed across the cell membrane but is concentrated in the foot processes adjacent to endothelial cells (Nielsen et al. 1997). This concentrate of channels in one part of the membrane is termed polarity. Although the concentration of AQP4 channels is greater at the foot processes than the rest of the cell, the absolute number of channels at the foot processes and at the rest of the cell is approximately the same. This arrangement suggests that water flows through the astrocyte, entering from the capillary via the foot process and exiting across the rest of the cell membrane into the extracellular space.

The mechanism of the formation of polarity is becoming clear. In the absence of endothelia (*e.g.* cultured astrocytes (Saadoun et al. 2005b), malignant astrocytes (Saadoun et al. 2002a; Warth et al. 2007), glial limitans and circumventricular organs

(Nielsen et al. 1997; Rash et al. 1998)) AQP4 re-distributes evenly throughout the astrocyte cell membrane. This suggests that endothelial cells signal astrocytes to polarise AQP4 expression in the cell membrane. AQP4 channels are anchored in the membrane by their C terminus, which can bind to PDZ domains implying localization of AQP4 by association with cytoskeletal proteins (Songyang et al. 1997). One of the proteins required to anchor AQP4 is α-syntrophin, a part of the dystrophin-associated protein complex (Neely et al. 2001). Mice lacking α-syntrophin lack astrocyte AQP4 polarity and respond to pathological stress in a similar way to AQP4 knockout mice (Amiry-Moghaddam et al. 2003; Neely et al. 2001). This provides strong evidence that AQP4 function is dependent on a polar membrane distribution.

AQP4 is also densely expressed at the glia limitans externa (separating brain and subarachnoid cerebrospinal fluid (CSF)), as well as ependymal cells and sub-ependymal astrocytes (separating brain and ventricular CSF) (Nielsen et al. 1997; Rash et al. 1998). AQP is therefore found at all the sites where water enters or exits the brain suggesting an important role in brain homeostasis.

The current knowledge of patterns of AQP4 expression is based on experiments using normal rodents in a steady physiological state. If necessary, alterations in AQP4 expression density could allow control over the rate of flow of water across a membrane. For example, an increase in AQP4 expression in the glia limitans compared with expression at the perivascular foot processes may limit oedema

formation across BBB and encourage drainage of oedema. Increased AQP4 expression is a common finding in disease in both humans and rodents.

There are several, often inconsistent, reports of altered AQP4 expression in different diseases. Such inconsistencies probably arise because of different AQP detection methods (mRNA versus protein), antibody specificities, tissue processing, species-specific responses and insult severities. In general, AQP4 expression is upregulated in astrocytes associated with brain oedema. For example, AQP4 over-expression in human astrocytomas correlates with the presence of brain oedema on magnetic resonance scans (Saadoun et al. 2002a; Warth et al. 2007). Correlations between AQP4 expression and brain oedema have been reported after brain ischaemia (Chen et al. 2007; Meng et al. 2004) and traumatic brain injury (Chen et al. 2007; M. C. Sun et al. 2003) in rodents. Such studies reinforce the notion that AQP4 plays an important role in the formation and/or absorption of brain oedema fluid. AQP4 expression also becomes upregulated in reactive astrocytes and reactive microglia (Auguste et al. 2007; Saadoun et al. 2005b), suggesting a possible role in glial scar formation. Overall, regulation studies provide only indirect evidence about the functions of AQP4 in the brain.

Very little research has been published on the role of AQP4 in SAH. Examination of human tissue after SAH has shown an increase in astrocyte expression of AQP4 yet the purpose and mechanism of this remains unclear (Badaut et al. 2003; Saadoun et al. 2003).

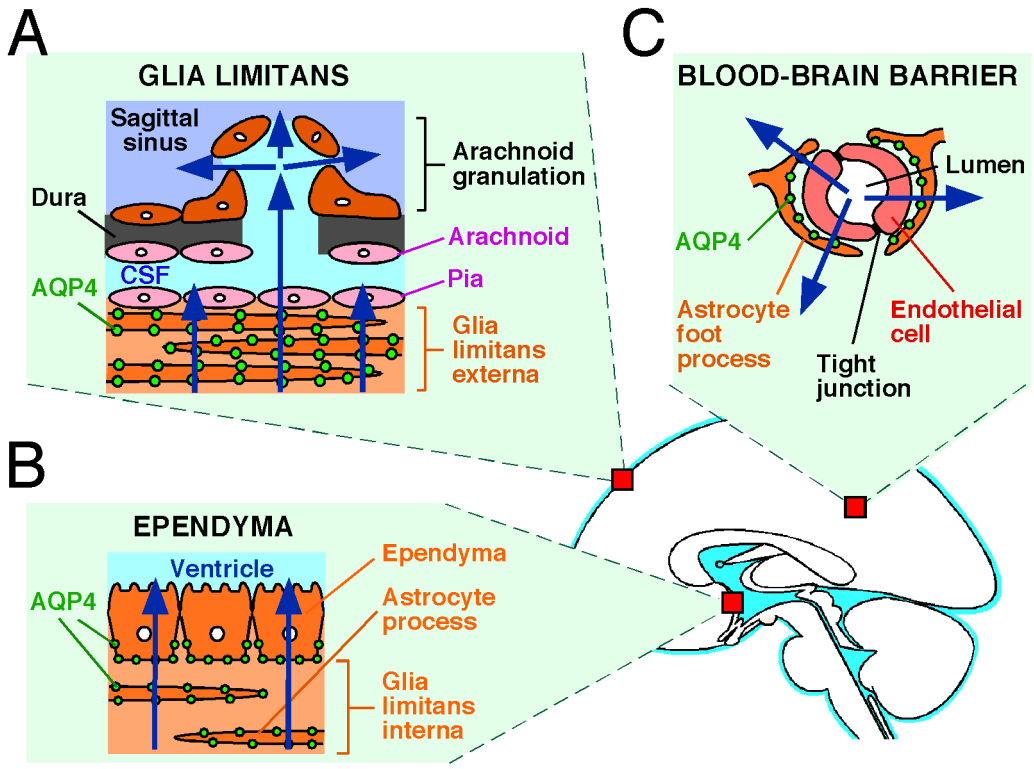

Figure 4. Locations of AQP4 expression. AQP4 is strongly expressed at each boundary between the brain and adjacent fluid spaces. [Adapted from Tait MJ *et al.* Water movements in the brain: role of aquaporins. *Trends Neurosci*. 2008 Jan;31(1):37-43.]

3.3 AQP4 function

AQP4 plays important roles in formation and resolution of brain oedema, astrocyte migration and regulation of neuronal activity. I will consider each in turn.

3.3.1. AQP4 and brain oedema. The pattern of distribution of AQP4 within the brain suggests that AQP4 controls water flow into and out of the brain. There is mounting evidence that AQP4 deficiency is associated with reduced cytotoxic brain oedema in mouse models, including water intoxication, focal cerebral ischaemia (Manley et al. 2000), and bacterial meningitis (Papadopoulos and Verkman 2005). For example, AQP4 -/- mice develop 35 % less hemispheric brain swelling than wildtype mice 24 h after middle cerebral artery occlusion (Manley et al. 2000). Reduced brain swelling after cerebral ischaemia and water intoxication has also been reported in α-syntrophin null mice, which have reduced AQP4 expression in astrocyte foot processes (Amiry-Moghaddam et al. 2003; Amiry-Moghaddam et al. 2004). Compared with wildtype mice, in AQP4 (Papadopoulos and Verkman 2005) and α-syntrophin (Amiry-Moghaddam et al. 2004) deficient mice the rate of water uptake into brain parenchyma after water intoxication is reduced 9-fold (Papadopoulos and Verkman 2005).

Water molecules moving from the blood via the BBB, into brain cross three cell membranes: luminal and basal endothelial membranes that lack AQPs, and the astrocyte foot process membrane that contains AQP4. Water moves across the endothelium by simple diffusion and vesicular transport, and across the astrocyte foot process primarily through AQP4 channels. These membranes are equivalent to three

resistors in series, with the astrocyte membrane resistance substantially increased in AQP4 deficiency.

Experiments using AQP4 over-expressing mice confirm that the AQP4 channels at the foot process are the limiting factor to the osmotic flow of water into the brain, not the endothelial cell membranes. In these mice M23 expression is driven by a GFAP promoter resulting in 2-3 fold over expression of AQP4 at the astrocyte foot processes. AQP4 over-expressing mice develop more cerebral oedema when exposed to water intoxication (Yang et al. 2008). AQP4 deficiency at the BBB therefore increases its resistance to water and leads to reduced formation of cytotoxic oedema.

In contrast to its beneficial role in cytotoxic oedema, AQP4 deficiency produces more brain swelling in mouse models of vasogenic oedema, including brain tumour, infusion of normal saline into brain extracellular space (ECS), and focal cortical freeze injury (that renders the BBB leaky) (Papadopoulos et al. 2004). Melanoma cells implanted in brains of wildtype and AQP4 -/- mice produce comparable tumours (~ 45 mm^3) after a week with higher intracranial pressures in AQP4 -/- mice (40 *vs.* 20 cmH_2O). These findings suggest that in vasogenic brain oedema, excess water enters brain ECS independent of AQP4, but exits the brain primarily through AQP4 water channels into the CSF and blood (Figure 3). This is a radical proposition because it implies that interstitial water is eliminated by an AQP4-dependent transmembrane route, rather than by bulk flow between cells as originally thought (Reulen et al. 1978; Tsuyumu et al. 1981). After kaolin injection into the cisterna magna, which causes obstructive hydrocephalus, AQP4 -/- mice developed

more severe hydrocephalus than wildtype mice (Bloch et al. 2006a). Reduced interstitial water clearance from brains of AQP4 -/- mice is consistent with the hydrodynamic theory of CSF flow (Greitz et al. 1997). According to this theory, excess interstitial fluid is eliminated by a trans-capillary (AQP4-rich) route into the blood rather than by bulk flow into the CSF and arachnoid granulations. The routes of water exit from the brain are shown in Figure 2

3.3.2 AQP4 and astrocyte migration. An unanticipated role for AQPs in facilitating cell migration was first reported for AQP1 and vascular endothelial cells in mice implanted with melanoma tumours (Saadoun et al. 2005a). Subsequent studies showed that lack of AQP slows migration speed two- to three-fold (Papadopoulos et al. 2008; Saadoun et al. 2005a; Saadoun et al. 2005b). Impaired migration in cultured AQP4 knockout and knockdown astrocytes has been demonstrated as has impaired glial scarring and astrocyte migration in AQP4 -/- mice *in vivo* (Saadoun et al. 2005b) (Auguste et al. 2007). There are two possible mechanisms of AQP4 involvement in astrocyte migration. The first is that once actin depolymerisation and ion transport have increased the intracellular osmolality in the leading edge, water enters through the cell membrane, via AQP4, increasing the local cytoplasmic pressure forming a cell membrane protrusion that allows the cell to advance. Actin then repolymerises to stabilize the protrusion. The second theory is that in migrating astrocytes, AQP4 facilitates transmembrane water movements, which are required to allow rapid changes in cell shape and volume to occur as the cell squeezes through the irregular extracellular space between stationary cells.

3.3.3. AQP4 and neuronal activity. In the 1990's, morphological studies showed co-localisation of AQP4 with the inward rectifying channel Kir4.1 in the retina leading to the idea that water and K^+ fluxes are coupled (Nagelhus et al. 1999). More recently, AQP4 -/- mice were found to have increased auditory brainstem evoked response thresholds (J. Li and Verkman 2001) and reduced electroretinographic potentials (J. Li et al. 2002). Compared with wildtype mice, AQP4 -/- mice have higher seizure threshold, but longer seizures in response to the convulsant pentylenetetrazol (Oshio et al. 2004), or hippocampal stimulation (Binder et al. 2006). There is also evidence of altered neurotransmitter release after high K^+ depolarization in AQP4 -/- mouse brain (Ding et al. 2007). Taken together, these studies suggest a major role for AQP4 in controlling neuronal activity.

There are two theories as to how a water channel can alter neuronal excitability. A functional association between AQP4-facilitated water movement and K+ movement through the Kir4.1 channel would lead to altered K+ kinetics in brain ECS and could account for the altered neuronal activity in AQP4 deficiency. Alternatively, increased ECS volume may raise the buffering capacity for K+ released into the ECS during neuronal excitation, preventing large changes in ECS [K+].

4.1 The AQP4 knockout mouse

Currently there are no known AQP4 inhibitors and therefore the roles of AQP4 in the brain have largely been defined using AQP4 -/- mice. Such mice were first generated at the University of California, San Francisco using targeted vector construction and embryonic stem cell screening (Ma et al. 1997). No AQP4 transcript is found by

Northern blot analysis nor is any AQP4 seen on immunocytochemistry in these mice (Ma et al. 1997). There is no increase in AQP1 or AQP9 mRNA levels indicating that there is no compensatory upregulation in AQP1 or AQP9 (Papadopoulos et al. 2004).

The phenotype of the resulting AQP4 -/- mouse is identical to the wildtype mouse on first inspection. Growth, body weight and lifespan are the same (Ma et al. 1997). AQP4 -/- mice have normal serum [Na^+] and osmolality, urine output (except for a slight defect in maximal urine concentrating ability) and temperature (Ma et al. 1997; Papadopoulos et al. 2004). Previous comparisons of CNS characteristics are summarized in **Table 1.**

Table 1. Published baseline CNS characteristics in AQP4 -/- mice generated originally by Ma *et al.* (1997)

Characteristic	**Assessment**	**Tissue**	**Effect of AQP4 deletion**	**References**
Cerebral vessels	Gross anatomy	Brain	No effect	(Manley *et al.*, 2000)
	Electron microscopy	Cerebral cortex	No effect	(Manley *et al.*, 2000, Papadopoulos and Verkman, 2005)
	Evans blue extravasation	Whole brain	No effect	(Papadopoulos *et al.*, 2004, Bloch *et al.*, 2005, Feng *et al.*, 2008)
Pressure-volume	Intracranial pressure	Whole brain	No effect	(Papadopoulos and Verkman, 2005)
	Intracranial compliance	Whole brain	No effect	(Papadopoulos and Verkman, 2005)
	Lateral ventricle volume	Brain	No effect	(Bloch *et al.*, 2006)
Extracellular space	Surface photobleaching	Cerebral cortex	Enlarged ECS	(Binder *et al.*, 2004b)
	Fibreoptic photobleaching	Many brain regions	Enlarged ECS	(Zador *et al.*, 2008)
	TMA+	Cerebral cortex	Enlarged ECS	(Yao *et al.*, 2008)
Other AQP expression	Real-time PCR	Whole brain	No effect	(Papadopoulos and Verkman, 2005)
Spinal cord	Vascular anatomy	Spinal cord at T6	No effect	(Saadoun *et al.*, 2008)
	White matter tract sizes			
	Myelination			

4.2 The Nanjing AQP -/- mouse

More recently, AQP4 -/- mice have been independently generated in Nanjing Medical University in China (Fan et al. 2005) using an identical gene targeting approach to that used to produce the San Francisco AQP4 -/- mice. Dr. Hu's group have reported that AQP4 deletion produced severe abnormalities in BBB permeability and reduced expression of the astrocyte marker GFAP in the 'Nanjing' mice (Zhou et al. 2008). They have also reported a series of other phenotypes in their mice, including subfertility (X. L. Sun et al. 2008), altered response to a variety of drugs including opiates (Wu et al. 2008), antidepressants (Kong et al. 2008), cocaine (Z. Li et al. 2006), MPTP (Fan et al. 2008), as well as markedly impaired neurotransmission involving dopamine, 5-hydroxytryptamine (Ding et al. 2007; Fan et al. 2005; X. L. Sun et al. 2007) and glutamate (Zeng et al. 2007).

These unexpected results have lead to much confusion amongst those who study AQP4. Before undertaking further experiments I felt it was important to characterize my AQP4 mice in detail.

5.1 Definition of subarachnoid haemorrhage

The subarachnoid space contains CSF and is located between the pia mater and the arachnoid mater. Haemorrhage into this space is referred to as subarachnoid haemorrhage (SAH). Most SAH is due to trauma however the pathophysiology, natural history and management of traumatic and non-traumatic (or spontaneous) SAH are so dissimilar that this thesis will not consider traumatic SAH further (Greene et al. 1995).

Spontaneous SAH most commonly occurs due to the rupture of an aneurysm causing the sudden release of blood at high pressure into the CSF (Rinkel et al. 1993). The incidence of SAH is about 10 people per 100 000 per year (de Rooij et al. 2007; Pobereskin 2001) and the overall mortality after SAH is estimated at 32 – 67 %(Hop et al. 1997). Furthermore, about 30% of survivors will have a moderate to severe disability (Hop et al. 1997).

5.2 SAH and cerebral oedema

The association between SAH and cerebral oedema has long been recognized (Goldberg and Handler 1960; Joynt et al. 1965). Despite this, the exact mechanism of oedema formation is yet to be elucidated. Both cytotoxoic and vasogenic oedema have been described after SAH. Rupture of an aneurysm results in a direct connection between the arterial and CSF spaces. This causes a rapid surge in ICP to equilibrate with the arterial pressure resulting in an intracranial circulatory arrest (Voldby and Enevoldsen 1982). This severe insult leads to a 'reflex triad' of early oedema, vasomotor paralysis and increased cerebral blood volume which keeps the ICP raised after the aneurysm has stopped bleeding (Grote and Hassler 1988). Oedema formation may therefore be biphasic: the initial rise in ICP and circulatory arrest results in cytotoxic oedema (Busch et al. 1998). The subsequent prolonged raised ICP leads to ischaemia and triggers the apoptotic cascade resulting in vasogenic oedema due to BBB dysfunction (Cahill et al. 2006). Other suggested mechanisms for oedema formation after SAH include: autoregulatory breakthrough, microvascular compromise causing ischaemia, aquaporin dysfunction and the cytotoxic effects of blood products (Claassen et al. 2002).

5.3 Clinical significance of cerebral oedema after SAH

Global brain oedema is evident on 6 – 8 % of initial CT scans after SAH (Claassen et al. 2002; Kassell et al. 1990; Lagares et al. 2001), although studies using diffusion-weighted MRI estimate a considerably higher incidence of brain oedema (Liu et al. 2007). Brain oedema is associated with a larger CSF blood load and a reduced level of consciousness at presentation (Claassen et al. 2002) and is an independent risk factor of mortality or poor functional outcome (Claassen et al. 2002; Lagares et al. 2001).

Experimental Procedures

6.1 AQP4 -/- mice.

AQP4 -/- mice with a CD1 genetic background were originally generated in Prof. Verkman's laboratory at the University of California at San Francisco (Ma et al. 1997). The mice used here were bred and genotyped in an approved facility at St. George's University of London. The experiments were performed after obtaining approval from the University of California at San Francisco Committee on Animal Research or the local research ethics committee and were authorised under the UK Home Office Animals (Scientific Procedures) Act 1986. Experiments were approved by the British Home Office. Weight-matched (30 – 35 g) male wildtype and AQP4 -/- mice with a CD1 genetic background, aged 8 – 10 weeks, were used in these experiments. The investigators were 'blinded' to mouse genotype during the experiments and data analysis. Mice were anesthetized using 2,2,2-tribromoethanol (Avertin, Sigma-Aldrich, Poole, UK) by injecting *i.p.* a 6.7 ml/kg bolus followed by 1.7 ml/kg every 20 min.

6.2 Numbers of WT and AQP4 -/- mice used

In total I used 124 mice. 24 were used for comparison of wildtype and AQP4 -/- mice. Brain tissue was obtained from 5 wildtype and 5 AQP4 -/- mice for comparisons of gross anatomy, immunohistochemistry for NeuN and GFAP, and myelination. Brain tissue from 3 wildtype and 4 AQP4 -/- (1 with streptococcal meningitis) mice was used for electron microscopy. A further 3 wildtype and 4 AQP4 -/- mice (1 with focal cortical freeze injury) were used for the comparative BBB permeability studies.

Experiments on cerebral oedema after SAH required 100 mice. 5 wildtype and 5 AQP4 -/- mice were used to characterize the animal model. Experimental SAH was given to 22 wildtype and 22 AQP4 -/- mice for subsequent measurement of intracranial pressure, brain water content and neurological score. 6 wildtype and 6 AQP4 -/- mice were used as controls for the comparison. Evans blue dye tests of BBB integrity were performed on 5 wildtype and 5 AQP4 -/- mice. Assessment of the permeability of the glia limitans to water required 11 wildtype and 11 AQP4 -/- mice. 2 wildtype mice were used to assess the response of AQP4 expression to SAH.

6.3 Tissue processing.

For light microscopy, mice were given a lethal dose of anaesthetic and perfusion-fixed through the left cardiac ventricle with 4% neutral buffered formaldehyde (Sigma, Poole, UK). The brain was removed, post-fixed in similar fixative overnight, and dehydrated through serial alcohols into paraffin wax. Serial coronal sections were cut starting at the frontal pole. Sections (7 μm thick) were collected at 1.600, 1.607, 1.614 and 2.800 mm. For electron microscopy, the mice were given a lethal dose of anaesthetic and were perfused through the heart with cacodylate buffer (0.1 M, pH 7.2–7.4) followed by 2.5% glutaraldehyde and 2% paraformaldehyde in cacodylate buffer at a constant pressure of 110 mm Hg, using a method adapted from Brown & Brierley (A. W. Brown and Brierley 1968). To reduce mouse-to-mouse variability, all brains were processed simultaneously using the same solutions.

6.4 Gross anatomy.

Coronal brain sections at 1.600 and 2.800 mm from the frontal pole were stained with Luxol Fast Blue (see myelin staining below) and examined in a BX-51 Olympus light microscope. I chose these sections because they provide a good view of the lateral and third ventricles. Digital photomicrographs were taken using the x10 objective under identical illumination settings. The captured images were stored in 8-bit jpg format and processed using ImageJ (v.1.40, http://rsb.info.nih.gov/ij/) to measure the cross-sectional area of each brain section, and of each lateral and 3rd ventricle. The tissue sections at 1.600 mm from the frontal pole were also used to quantify myelination (see below).

6.5 Immunohistochemistry.

Coronal brain sections at 1.607 mm from the frontal pole were immunostained using a primary antibody against the neuronal nuclear marker NeuN (1:200, mouse monoclonal, Cat No. MAB377, Millipore, Livingstone, UK). Coronal sections at 1.614 mm from the frontal pole were immunostained with the astrocyte specific marker Glial fibrillary acidic protein (GFAP) (1:200, rabbit polylonal, Cat. No. AB5804, Millipore, Livingstone, UK). Secondary antibodies were biotinylated anti-mouse (for NeuN) and biotinylated anti-rabbit (GFAP) at 1:1,000 dilution (Vector Labs, Peterborough, UK). Immunoreactivity was visualized brown by incubation with avidin-HRP and DAB / H_2O_2. Counterstaining was with hematoxylin.

6.6 Myelin staining.

Coronal brain sections were stained using the myelin-specific dye Luxol Fast Blue as previously described (Saadoun et al. 2008). Briefly, the coronal brain sections at 1.600 mm from the frontal pole were deparaffinised, rehydrated and incubated in 0.1% Luxol Fast Blue (in 95% alcohol and 0.5% acetic acid) (Sigma, Poole, UK) solution at 40°C overnight. After rinsing excess stain with 95% ethanol and washing in distilled water, slides were immersed in 0.05% lithium carbonate solution for 30 s. Sections were then dehydrated in serial alcohols, and mounted in VectaMount mounting medium (Vector Labs, Peterborough, UK).

6.7 Analysis of NeuN staining.

To standardize measurements, I arbitrarily chose to analyze the lateral cerebral cortex at 1.607 mm from the frontal pole. The cortical thickness was measured at this site. A grid composed of ten 100 × 50 μm rectangles was then superimposed on each brain section and was used to determine the neuronal and total (neuronal + non-neuronal) nuclear surface densities at different distances (0 – 0.5 mm) from the brain surface.

6.8 Analysis of GFAP staining

GFAP expression was estimated semi-quantitatively after immunohistochemistry. Photomicrographs (8-bit jpeg format) of GFAP-immunostained tissue were taken using the same microscope settings for all sections (x40 objective, illumination 10, exposure 105 ms). ImageJ was used to quantify GFAP immunoreactivity around microvessels as brightness minus background staining, within a 20 μm radius around 20 randomly selected microvessels in each mouse cerebral cortex. To quantify GFAP

immunoreactivity at the glia limitans, I measured the brightness of immunostaining minus background down to 30 μm from the brain surface in 10 μm intervals.

6.9 Analysis of myelin staining

To quantify myelination, I selected the corpus callosum, which is one of the most prominently stained white matter tracts. A digital image of the middle portion of the corpus callosum (8-bit jpeg format) was taken using the same microscope settings for all sections (x10 objective, illumination 10, exposure 50 ms). Myelination was quantified using two parameters, the thickness (*t*) at different distances (*d*) from the midline, as well as the staining intensity (*i*) in the midline portion of the corpus callosum.

6.10 BBB permeability

BBB permeability was assessed by injecting HRP (Type VI, Sigma, Poole, UK) diluted in normal saline (10 mg/mL) into the internal jugular vein (200 μL/mouse). Ten minutes after injection, mice were decapitated and the brain was removed and fixed in 2 % glutaraldehyde in PBS overnight. The brain was cryoprotected in 30% sucrose in PBS until it sank, and then embedded in OCT (R.A. Lamb Ltd, Eastbourne, UK). Serial coronal frozen sections (50 μm thick) were cut every 200 μm from the frontal pole and HRP was visualized brown by incubation with DAB / H_2O_2. For comparison, I performed focal cortical freeze injury in one AQP4 -/- mouse to damage the BBB as described (Papadopoulos et al. 2004). Six hours after the injury, I injected HRP and processed the brain as described above.

6.11 Electron microscopy

Immediately after perfusion fixation, the brain was rapidly removed, rinsed in cacodylate buffer, post-fixed in 1% osmium tetroxide in cacodylate buffer for 2 h, and rinsed again in cacodylate buffer. The tissue was then immersed in 30% ethanol containing 2% uranyl acetate for 30 min before being dehydrated through ascending alcohols and processed into Spur's resin (Agar Scientific, Stansted, Essex, UK). Ultrathin sections (80–90 nm) were then cut, picked up on 200 mesh copper grids, stained with lead citrate and viewed in a Hitachi H-7100 transmission electron microscope. Digital images (20 per mouse) were captured with a GATAN 689 CCD camera and Digital Micrograph software (Gatan Ltd., Corby, UK) from the frontal cortex and the caudate nucleus. Each picture contained a microvessel in cross section. Photomicrographs were also taken of 5 microvessel endothelial cell tight junctions per mouse. In total, I examined 60 microvessels and 15 tight junctions from wildtype as well as 60 microvessels and 15 tight junctions from AQP4 -/- mice. For comparison, I induced streptococcal meningitis in one AQP4 -/- mouse to produce perimicrovessel oedema as described (Papadopoulos and Verkman 2005). 24 h hours after the injury, the brain was processed as described above.

6.12 Induction of SAH. Anaesthetized mice were immobilized in a stereotactic frame (myNeurolab, St Louis, MO). Rectal temperature was maintained at 37 – 38 ºC using a heat lamp **(Figure 5)**. A midline scalp incision was made and two 0.8 mm diameter burr holes were drilled using a Foredom drill (Bethel, CT), 3 mm left of the bregma on the coronal suture, and immediately posterior to the right vein **(Figure 6)**. Autologous venous blood (30 µl) was withdrawn from the tail, heparinised, and

injected through a 27 G needle inserted through the anterior burr hole at 30º pointing posteriorly. The blood was injected over 7.5 s using a syringe driver (IVAC, San Diego, CA). ICP was monitored through the right-sided burr hole. After injection, the needle was left *in situ* for 10 min to prevent back flow. Once the needle and ICP monitor were removed, both burr holes were plugged with bone wax (Eastbourne DGH pharmaceuticals, Eastbourne, UK) and the scalp was sutured.

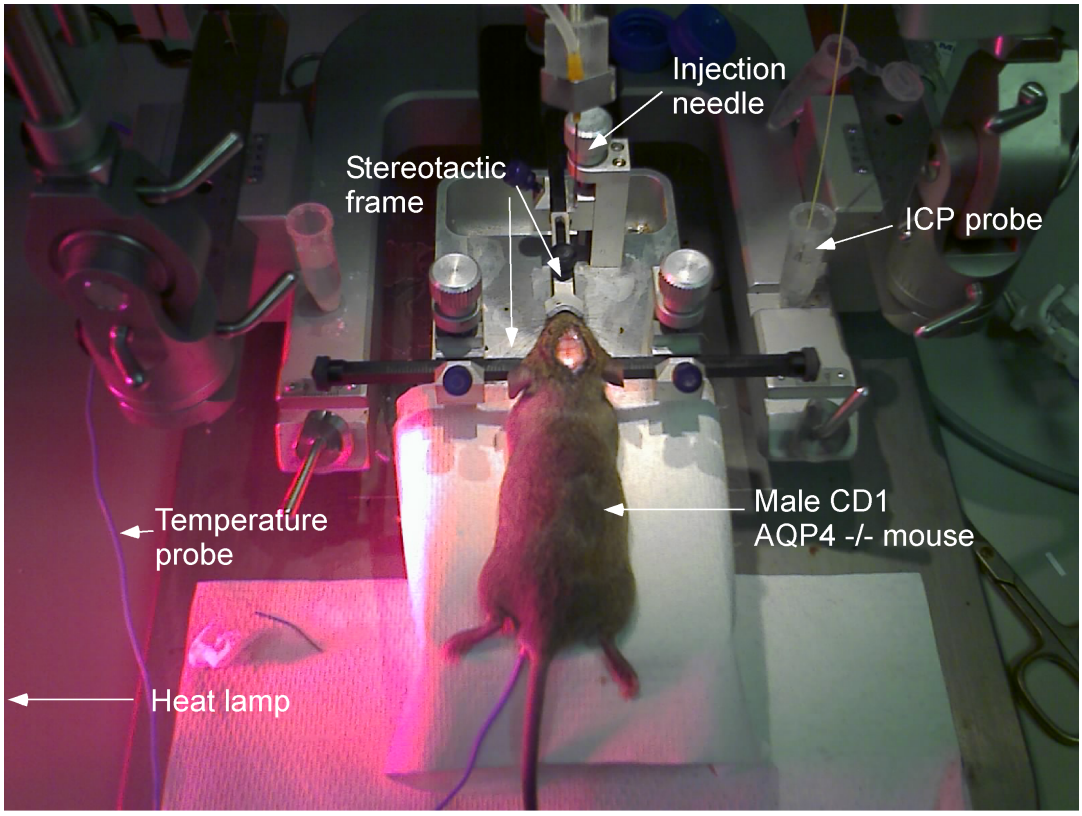

Figure 5. Mouse SAH model – set up. The anaesthetised mouse is held in a stereotactic frame with the sidebars set to 15mm and the mouth bar at 20mm. Temperature was measured *per rectum*. A heat lamp was used to prevent cooling. A midline scalp incision has been made, exposing the calvarium. The sagittal and coronal sutures can be seen.

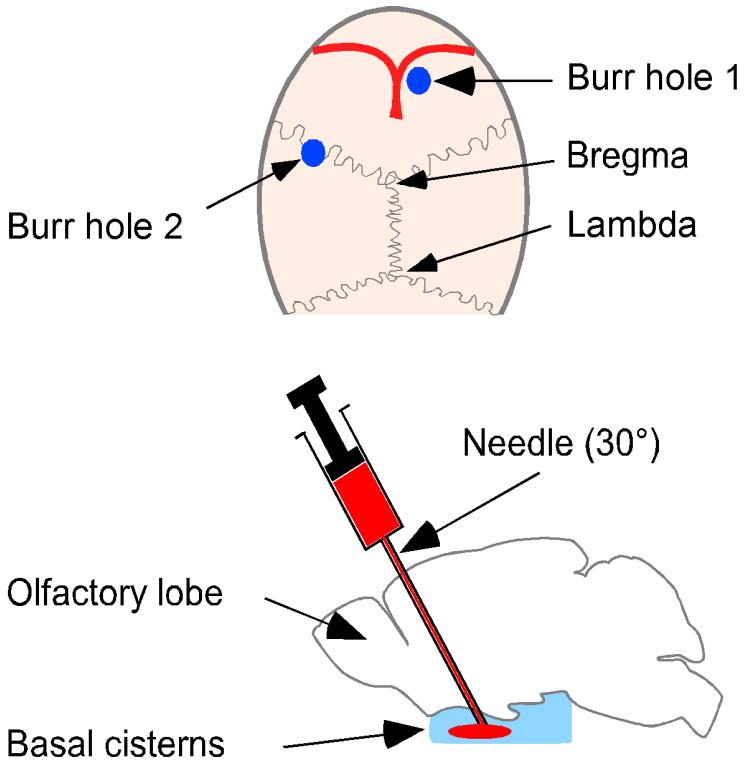

Figure 6. Mouse SAH model - injection. (Top) Mouse calvarium. Burr hole 1 is for injection and burr hole 2 for ICP monitoring. (Bottom) The injecting needle is advanced 30° to the perpendicular into the basal cisterns.

[Adapted from Tait MJ *et al.* Increased brain oedema after subarachnoid hemorrhage in *aqp4*-null mice. *Neuroscience.* 2010 Apr 28;167(1):60-7.]

6.13 Measurement of ICP. An ICP monitoring micro-probe (SPC-320; Millar, Houston, TX) was used. ICP recordings were taken using a computer interface (MP 35; Biopac, Santa Barbara, CA) throughout the injection of blood. Mice also had ICP monitoring for 10 min at 6 or 24 h after surgery.

6.14 Measurement of brain water content. Mice were killed by anaesthetic overdose and the brain was rapidly removed. Brains were weighed (w_1), placed in an oven (95 ºC, 48 h) and re-weighed (w_2). Percent brain water content was computed as $100 \times [1 - (w_1 - w_2) / w_1]$. Comparisons between AQP4 -/- and wildtype mice were made at 6 and 24 h after SAH.

6.15 Neurological assessment. I used a standard neurological scale (5 – 27 points), previously used for assessing mice after SAH (Parra et al. 2002) **(Figure 7)**.

Motor score

	0	1	2	3
Activity (5 min in open field)	No movement	Moves, no walls approached	1-2 walls approached	3-4 walls approached
Limb symmetry (suspend by tail)	No movement	Minimal movement	Abnormal forelimb walk	Symmetrical extension
Climbing (on inverted metal mesh)	Fails to hold	Holds < 4 sec	Holds, no displacement	Displaces across mesh
Balance (on 2cm diameter rod)	Falls < 2 sec	Falls > 2 sec	Holds, no displacement	Displaces across rod

Sensory score

	1	2	3
Proprioception (cotton tip to neck)	No reaction	asymmetrical head turning	Symmetrical
Vibrissae (cotton tip to vibrissae)	No reaction	Asymmetrical head turning	Symmetrical head turning
Visual (tip toward each eye)	No reaction	Unilateral blink	Bilateral blink
Olfactory (lemon juice on tip)	No sniffing	Brief sniff	Sniff > 2 sec
Tactile (needle stick to palm)	No reaction	Delayed withdrawal	Immediate withdrawal

Figure 7. Neurological examination variables. Taken from *Mouse model of subarachnoid haemorrhage and vasospasm: Augusto Parra* et al 2002 (Parra et al. 2002). Each mark is summed to give a total of 5-27.

6.16 Assessment of BBB permeability. I sought qualitative and quantitative evidence of increased BBB permeability, the hallmark of vasogenic oedema formation. 2 MDa FITC-dextran and 10 kDa Rhodamine-dextran (0.2 mL of 25 mg/ml in 0.9 % saline each, Sigma-Aldrich, Poole, UK) were injected into the internal jugular vein. After 30 min the mice were killed, the brains were extracted, fixed in formalin, cryoprotected in 30 % sucrose and embedded in OCT (Raymond Lamb, Eastbourne, UK). Frozen sections (7 μm thick) of cerebral cortex distant from the needle and ICP monitoring sites was inspected using a BX-51 Olympus microscope.

The Evans blue dye (EBD) assay was used to quantify BBB opening. Mice were anaesthetized and EBD (4% in saline, 160 mg/kg; Sigma-Aldrich, Poole, UK) was injected into the right jugular vein. After 30 min the left cardiac ventricle was perfused with 30 ml 0.9 % saline. Brains were removed and placed in 2 ml N,N-dimethylformamide (Sigma-Aldrich, Poole, UK) at 55 ºC overnight. The concentration of extracted EBD in formamide was calculated by comparing optical absorbance at 610 nm against EBD-formamide standards **(Figure 8)**.

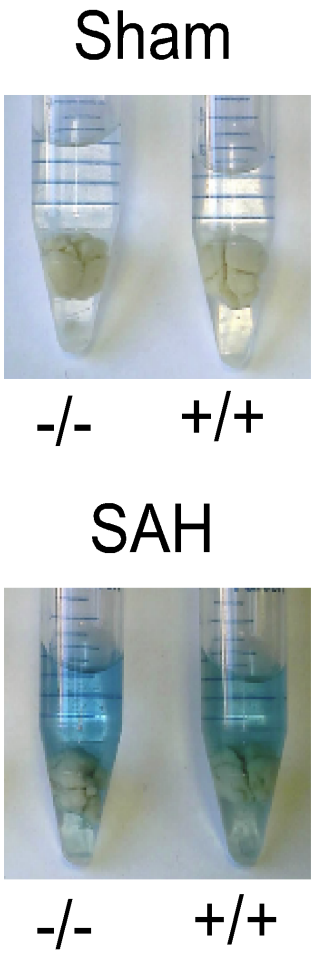

Figure 8. Mouse brains in formamide. Wildtype (+/+) and AQP4 -/- (-/-) mice had needle insertion (Sham) or SAH.

[Adapted from Tait MJ *et al.* Increased brain oedema after subarachnoid haemorrhage in *aqp4*-null mice. *Neuroscience.* 2010 Apr 28;167(1):60-7.]

6.17 Assessment of glia limitans osmotic permeability. A major route of oedema elimination is across the aqp4-rich glia limitans into the CSF(Marmarou et al. 1994; Reulen et al. 1977). To estimate glia limitans osmotic permeability, a right-sided craniectomy was performed. Craniectomy margins were the coronal suture interiorly, neck muscles posteriorly, capital suture medially, and 4 mm from the midline laterally **(Figure 9A)**. After carefully removing the dura, a cylinder (5 mm diameter, 3 mm high) of 4 % agarose in water (hypotonic) or normal saline (isotonic) was placed over the brain surface for 30 min, in a humid atmosphere **(Figure 9B)**. Mice were killed and the % water content of the right minus left cerebral hemisphere was determined.

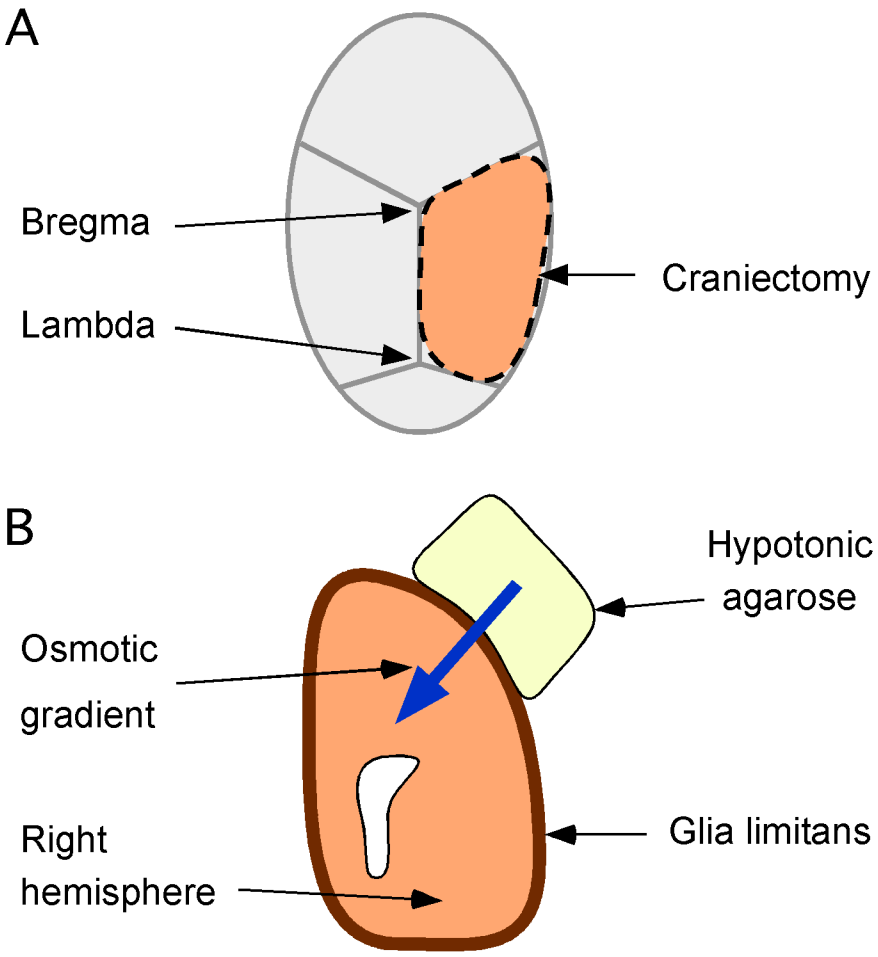

Figure 9. Assessment of glia limitans permeability to water. A. Craniectomy margins. **B.** Establishment of an osmotic gradient across the glia limitans. [Adapted from Tait MJ *et al.* Increased brain oedema after subarachnoid haemorrhage in *aqp4*-null mice. *Neuroscience.* 2010 Apr 28;167(1):60-7.]

6.18 Effect of SAH on AQP4 expression – histology. Brains were fixed in formalin, dehydrated in alcohols, and embedded in paraffin. Sections (7 μm thick) were deparaffinised, unmasked in citrate and exposed to a polyclonal rabbit anti-rat aqp4 antibody (Millipore-Chemicon, Watford, UK) followed by biotinylated goat anti-rabbit antibody (Vector Labs, Peterborough, UK) and streptavidin-HRP. Aqp4 immunoreactivity was visualized brown with DAB/H_2O_2. To visualize the ventricles, coronal brain sections at 2.8 mm from the frontal poles were stained with hematoxylin-eosin.

6.19 Statistical analysis. Parametric data, presented as Mean ± SEM, were compared using the Student *t* test or ANOVA as appropriate. Non-parametric data, shown as median, were compared using the Mann Witney U test. WinSTAT (v2001.1, A-Prompt, Lehigh Valley, PA) was used. Significance was taken to be $P < 0.05$.

Results

Before starting experiments to determine the role of AQP4 in SAH oedema, I undertook a detailed study of baseline brain characteristics in 'San Francisco' AQP4 -/- *vs*. wildtype. I wanted to be certain that none of my subsequent results with SAH could be explained by baseline differences. In order to exclude baseline differences of particular importance to the study of cerebral oedema I decided to assess both brain structure, which I divided into gross morphology (7.1) and microstructure (7.2), and the ultrastructure and function of the BBB (7.3).

7.1 Gross brain morphology.

To exclude differences in gross brain morphology I measured baseline brain and ventricular sizes.

7.1.1 Brain size.

I measured brain dimensions to exclude macroscopic differences in brain structure. As the brain has an irregular shape I took my measurements at two points a fixed distance from the frontal pole. I found no significant difference in coronal brain cross-sectional area between wildtype and AQP4 -/- mice at 1.600 mm or 2.800 mm from the frontal pole **(Figure 10)**. There was also no significant difference between wildtype and AQP4 -/- mouse brains in maximal width and maximal height of the brain in these coronal sections.

7.1.2 Ventricular size

A difference in the size of the ventricular system would result in a difference in the volume of neural tissue in two brains with the same external dimensions. I compared the size of both the lateral and third ventricles to exclude this possibility. The ventricles also have an irregular shape so I again measured the cross sectional area at a constant distance from the frontal pole to allow accurate comparison.

The lateral and 3rd ventricles were present in all coronal brain sections at 2.800 mm from the frontal poles. **Figures 11 and 12** show typical photomicrographs of the lateral and 3rd ventricles from a wildtype and an AQP4 -/- mouse brain. The two lateral ventricles, seen on either side below the corpus callosum, contained choroid plexus and were triangular superiorly with a thin inferior portion. In both wildtype and AQP4 -/- mice, the opposite walls of each lateral ventricle were adherent to each other in places. The 3rd ventricle, found in the midline, also contained choroid plexus and was of comparable shape in wildtype and AQP4 -/- mice. There were no significant differences between wildtype and AQP4 -/- mice in the cross-sectional areas of the lateral or 3rd ventricles in sections 2.800 mm from the frontal pole.

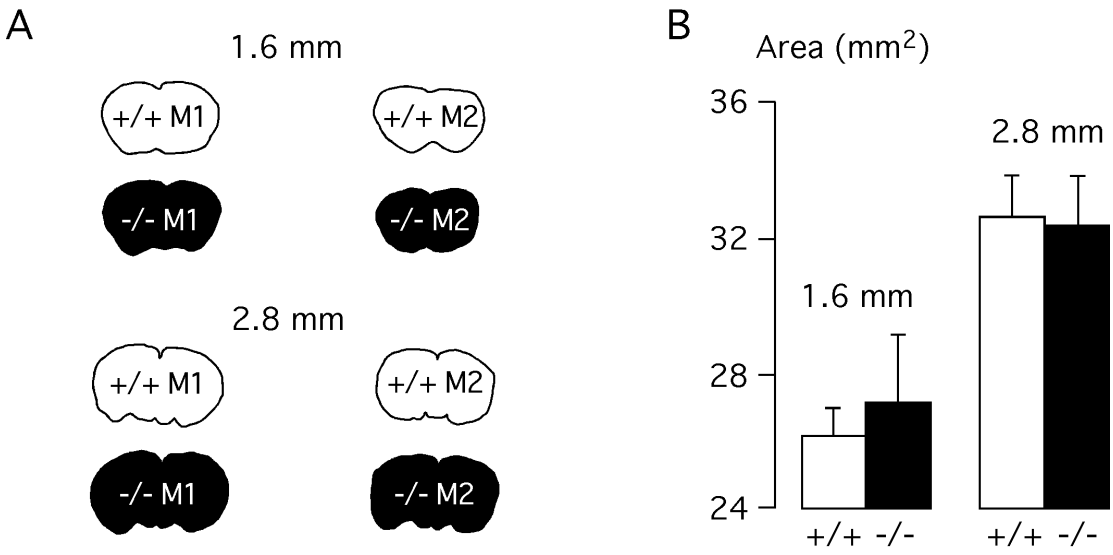

Figure 10. Gross brain morphology – brain size. A. Schematic of coronal sections of 2 wildtype (+/+) *vs.* 2 AQP4 -/- (-/-) mouse brains at 1.600 and 2.800 mm from the frontal pole. **B.** Cross sectional areas (mean ± SEM). The difference between wildtype (+/+) and AQP4 -/- (-/-) is not significant.

[Adapted from Saadoun S, Tait MJ *et al.* AQP4 gene deletion in mice does not alter blood-brain barrier integrity or brain morphology. *Neuroscience.* 2009 Jul 7;161(3):764-72.]

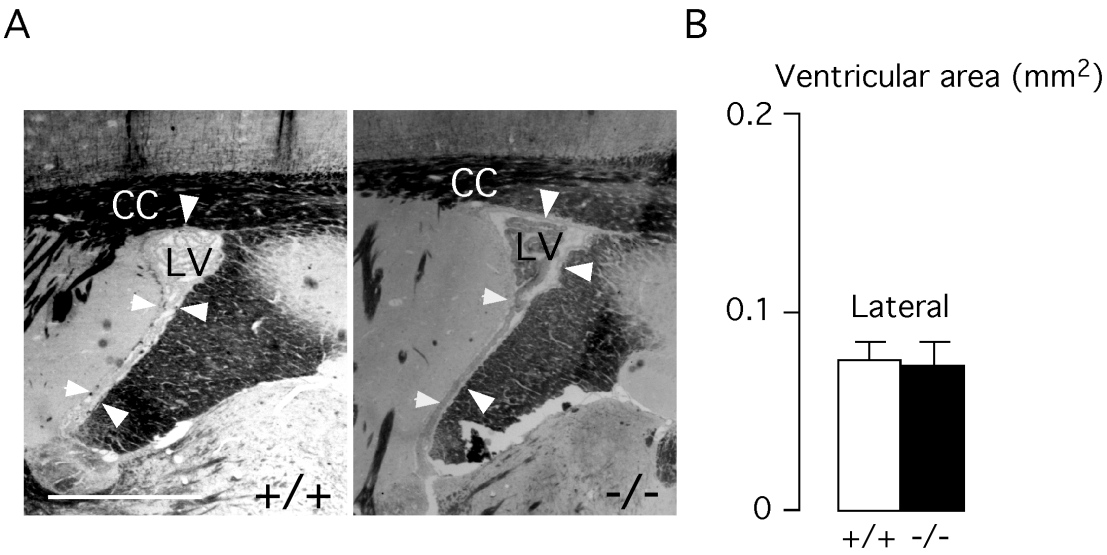

Figure 11. Gross brain morphology – lateral ventricle. A. Representative coronal sections (2.800 mm from frontal pole) with arrowheads indicating the left lateral ventricle in wildtype (+/+) and AQP4 -/- mice. **B.** Ventricular size measurements in 5 wildtype (+/+) *vs.* 5 AQP4 -/- (-/-) mice (mean ± SEM). The difference between wildtype (+/+) and AQP4 -/- (-/-) is not significant.

CC, corpus callosum; LV, lateral ventricle; bar = 0.5 mm.

[Adapted from Saadoun S, Tait MJ *et al.* AQP4 gene deletion in mice does not alter blood-brain barrier integrity or brain morphology. *Neuroscience.* 2009 Jul 7;161(3):764-72.]

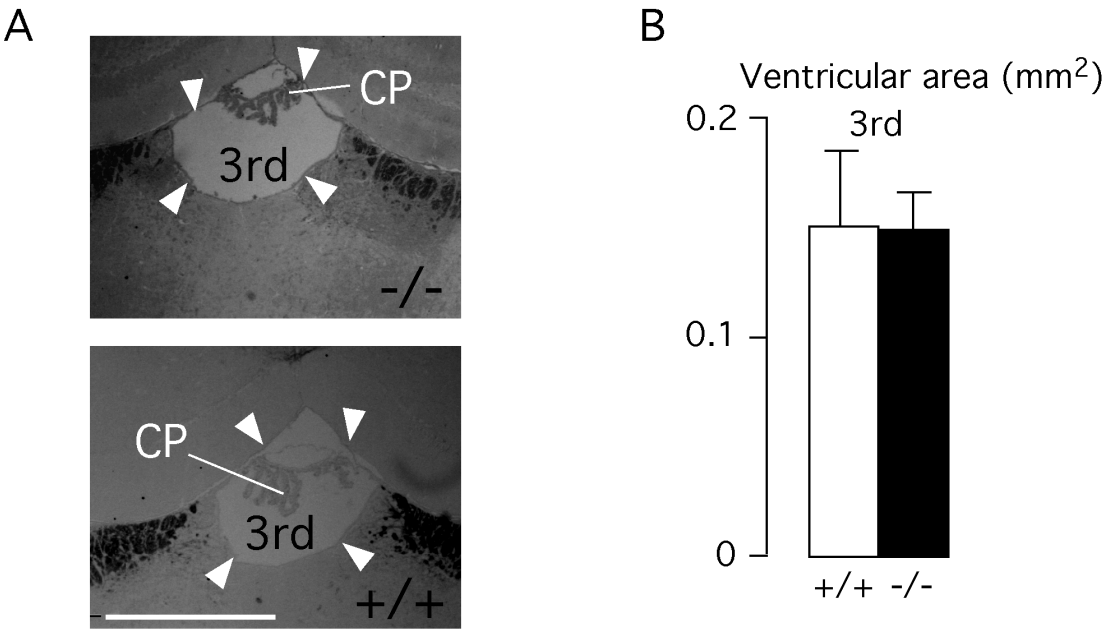

Figure 12. Gross brain morphology – third ventricle. A. Representative coronal sections (2.800 mm from frontal pole) with arrowheads indicating the 3rd ventricle. **B.** Ventricular size measurements in 5 +/+ *vs.* 5 -/- mice (mean ± SEM). The difference between wildtype (+/+) and AQP4 -/- (-/-) is not significant.

3rd, third ventricle; CP, choroid plexus; bar = 0.5 mm.

[Adapted from Saadoun S, Tait MJ *et al.* AQP4 gene deletion in mice does not alter blood-brain barrier integrity or brain morphology. *Neuroscience.* 2009 Jul 7;161(3):764-72.]

7.2 Microstructure

Brain consists of white matter, which predominantly contains neuronal axon tracts and glia, and grey matter, which predominantly contains the cell bodies of neurons and glial cells. I compared each in turn (7.2.1 and 7.2.2). I then focused in particular on the density of astrocyte populations as these cells are vital to brain water homeostasis (7.2.3).

7.2.1 White matter

To assess the white matter I studied the thickness and the degree of myelination of the white matter tracts. I assessed tract thickness because it is a reflection of the number of axons in the tract. Axonal myelination is vital to neuronal function and, also, the degree of myelination will alter the thickness of a tract for a given number of axons.

I used Luxol Fast Blue dye, which specifically stains myelin, to analyse the white matter tracts. I assessed each major white matter tract but used the corpus callosum for quantification as it is the largest and easiest to locate of the white matter tracts. Similar intense blue staining was evident in all major white matter tracts in wildtype and AQP4 -/- mice, with little or no staining of gray matter. **Figure 13** shows representative photomicrographs of the corpus callosum stained with Luxol Fast Blue in 3 wildtype and 3 AQP4 -/- mice. I found no detectable difference in the thickness (t) of the corpus callosum at different distances (d) from the midline between 5 wildtype and 5 AQP4 -/-mice (Fig. 4B). The Luxol Fast Blue staining intensity (i) in

the middle portion of the corpus callosum was not significantly different between wildtype and AQP4 -/- mice **(Figure 14)**.

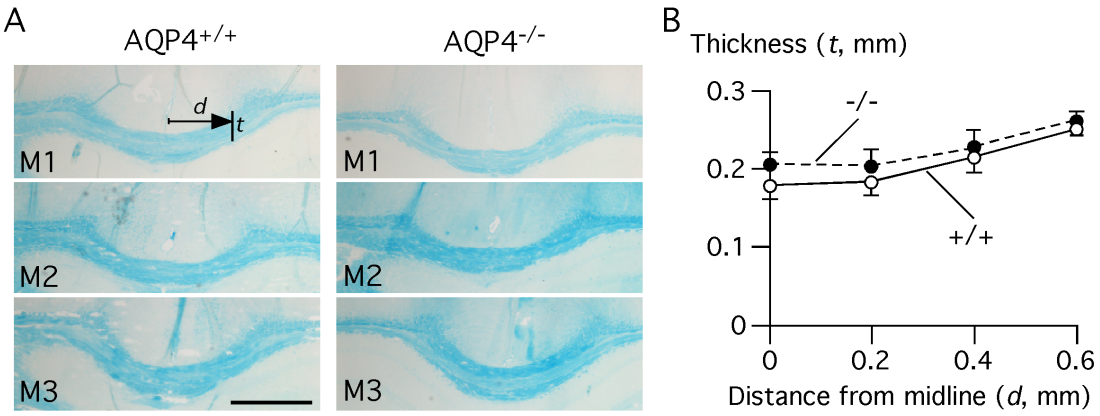

Figure 13. Myelination – corpus callosum thickness. A. Coronal sections (1.600 mm from frontal pole) stained with Luxol Fast Blue dye showing the corpus callosum. The micrographs were used to measure the corpus callosum thickness, *t*, at different distances *d* (0, 0.2, 0.4 and 0.6 mm), from the midline. **B.** Plot of *t vs. d* in 5 wildtype (+/+) and 5 AQP4 -/- (-/-) mice (mean ± SEM). The differences between wildtype and AQP4 -/- are not significant. Bar **(A)** = 0.5 mm.

[Adapted from Saadoun S, Tait MJ *et al.* AQP4 gene deletion in mice does not alter blood-brain barrier integrity or brain morphology. *Neuroscience.* 2009 Jul 7;161(3):764-72.]

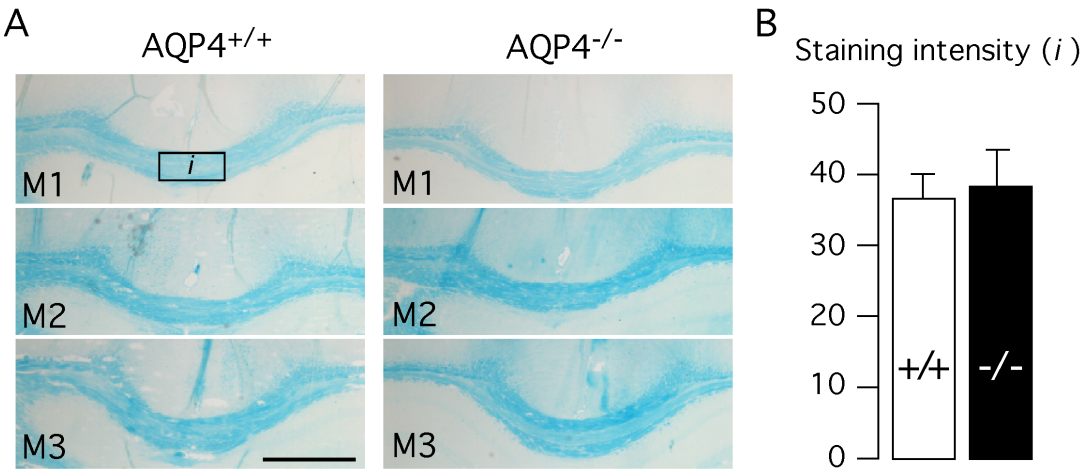

Figure 14. Myelination – staining intensity. A. Coronal sections (1.600 mm from frontal pole) stained with Luxol Fast Blue dye showing the corpus callosum. The micrographs were used to measure the mean blue staining intensity, *I*, within the boxed area. **B.** Plot of myelin staining intensity, *I*, in 5 wildtype and 5 AQP4 -/- (-/-) mice (mean ± SEM). The difference between wildtype and AQP4 -/- (-/-) is not significant. Bar **(A)** = 0.5 mm.

[Adapted from Saadoun S, Tait MJ *et al.* AQP4 gene deletion in mice does not alter blood-brain barrier integrity or brain morphology. *Neuroscience.* 2009 Jul 7;161(3):764-72.]

7.2.2 Grey matter

Grey matter contains both neuronal and glial cell bodies. I compared the density and distribution of both. The cellular architecture of cerebral cortex varies by Brodmann area so I standardized the brain region in each mouse by using coronal brain sections at 1.607 mm from the frontal pole in each case. I stained the tissue with NeuN, which is an antibody to a neuron specific nuclear protein found in vertebrates and present in nearly all subtypes of neuron in the mouse brain (Mullen et al. 1992). Counterstaining of non-neuronal cell nuclei with haematoxylin allows assessment of both neuronal and glial nuclear density within the cerebral cortex.

Following immunolabelling of NeuN, the neuronal nuclei appeared brown and the non-neuronal nuclei, counterstained with haematoxylin, appeared blue. The lateral cortical thickness in coronal section was 0.632 ± 0.064 mm in wildtype *vs.* 0.631 ± 0.065 mm in AQP4 -/- mouse brain. In wildtype and AQP4 -/- mice there are no NeuN immunopositive nuclei in the layer I of the cortex (down to ~100 μm from the pial surface) with a peak for neuronal nuclear density in layer II at around 200 – 250 μm. Layers III – VI were indistinct in this part of the cerebral cortex. The distribution of NeuN+ nuclei at different depths from the brain surface was similar in wildtype and AQP4 -/- mice. Layer I of the cortex (0 – 100 μm) contained several blue (non-neuronal) nuclei mostly in vascular endothelial cells. The overall ratio of neuronal: non-neuronal nuclei was about 1:1. The total (neuronal + non-neuronal) nuclear density at different distances from the brain surface did not differ significantly between wildtype and AQP4 -/- mice **(Figure 15).**

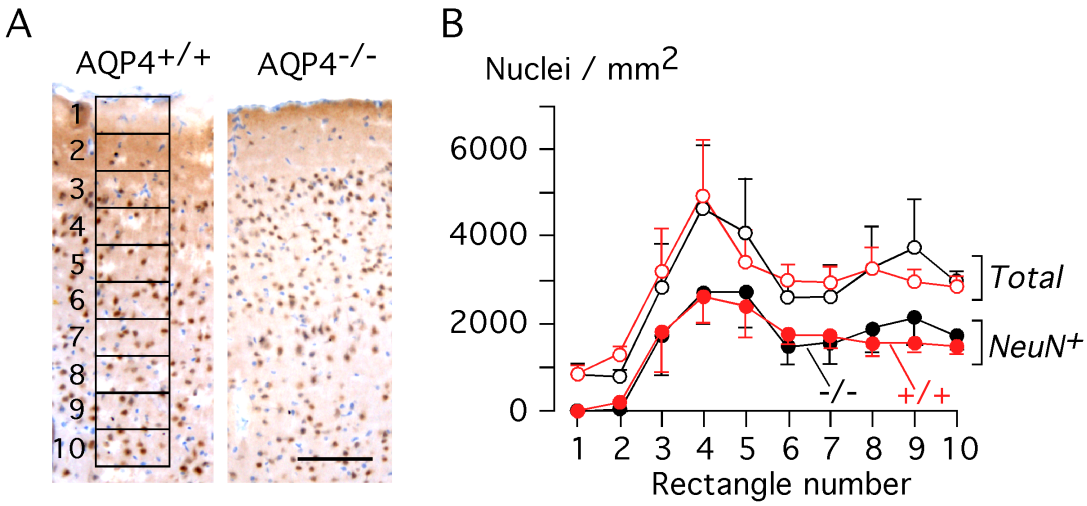

Figure 15. Neuronal (and non-neuronal) nuclear density. A. Coronal sections (1.607 mm from frontal pole) immunostained with the neuronal nuclear marker NeuN and counterstained with hematoxylin. I counted the number of neuronal (brown) and non-neuronal (blue) nuclei ten 100 μm × 50 μm rectangles. **B.** Nuclear density (*NeuN*$^{+}$, *Total*) at different distances from the brain surface in 5 +/+ (red) *vs.* 5 -/- (black) mice (mean ± SEM). Differences between +/+ and -/- mice are not significant. Bar = 100 μm (**A**). [Adapted from Saadoun S, Tait MJ *et al.* AQP4 gene deletion in mice does not alter blood-brain barrier integrity or brain morphology. *Neuroscience.* 2009 Jul 7;161(3):764-72.]

7.2.3 Grey matter astrocyte density

The distribution of astrocytes is of particular importance to the study of cerebral oedema as these are the cells that express AQP4. I therefore compared the density of astrocytes in two places vital to the role of AQP4 in cerebral oedema: the BBB and the glia limitans.

I stained for GFAP, which is an intermediate filament protein that, within the CNS, is specific to astrocytes. I chose GFAP primarily because it is commonly used as a histological marker for astrocytes. At the BBB, GFAP null mice have been shown to have abnormal structure implying a role for GFAP in BBB integrity(Goss et al. 1991). Furthermore, Zhou *et al.* reported a marked reduction in perivascular GFAP expression in the Nanjing AQP4 -/- mouse. Astrocyte density is vital to the structure of the glia limitans. This dense cellular sheet is important to current theories to explain differences in oedema elimination in AQP4 -/- mice. I therefore analysed GFAP expression at both the BBB and the glia limitans.

I found GFAP around microvessels, corresponding to the position of astrocyte foot processes, throughout the brains of wildtype and AQP4 -/- mice. **Figure 16** shows four representative microvessels from wildtype and four microvessels from AQP4 -/- mouse cerebral cortex. Although I found considerable variability in GFAP imunoreactivity between individual vessels I did not find a significant difference in cerebral cortical perimicrovascular GFAP immunoreactivity between wildtype and AQP4 -/- mice. There was also no significant difference in perimicrovascular GFAP

immunoreactivity in the corpus striatum between 5 wildtype and 5 AQP4 -/- mice (data not shown).

Figure 17 shows GFAP expression in 2 wildtype and 2 AQP4 -/- mice throughout the glia limiting membrane, at the surface of the brain. GFAP staining intensity increased strongly at the brain surface. There was no significant difference in the GFAP immunostaining profiles of the glia limitans between wildtype and AQP4 -/- mice.

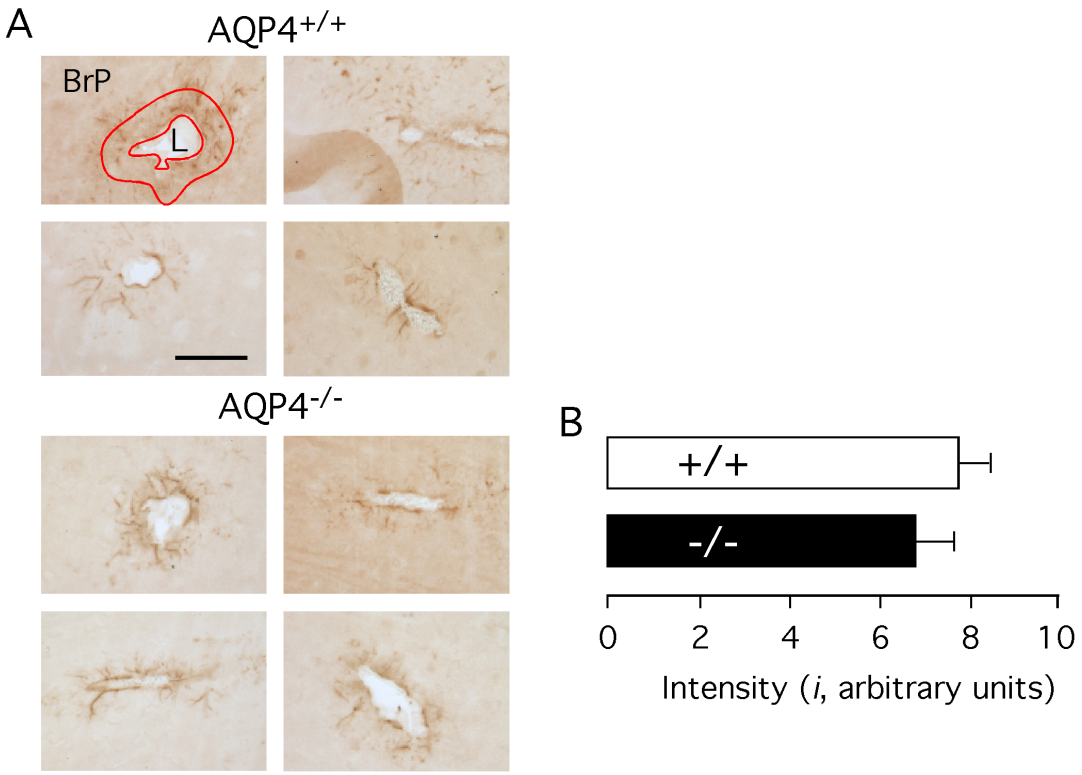

Figure 16. GFAP expression – perivascular. A. GFAP immunostaining (brown) around cerebral cortex microvessels from 5 +/+ and 5 -/- mice. Red contours indicate 20 μm border around the microvessel that was used to quantify GFAP expression. **B.** Quantification of perimicrovessel GFAP immunostaining. '*i*' is defined as the mean staining intensity 20 μm around microvessels minus the mean background staining. Values were measured from 5 +/+ *vs.* 5 -/- mice (20 microvessels per mouse, mean ± SEM). The differences between +/+ and -/- are not significant. Bar = 50 μm (**A**). [Adapted from Saadoun S, Tait MJ *et al.* AQP4 gene deletion in mice does not alter blood-brain barrier integrity or brain morphology. *Neuroscience.* 2009 Jul 7;161(3):764-72.]

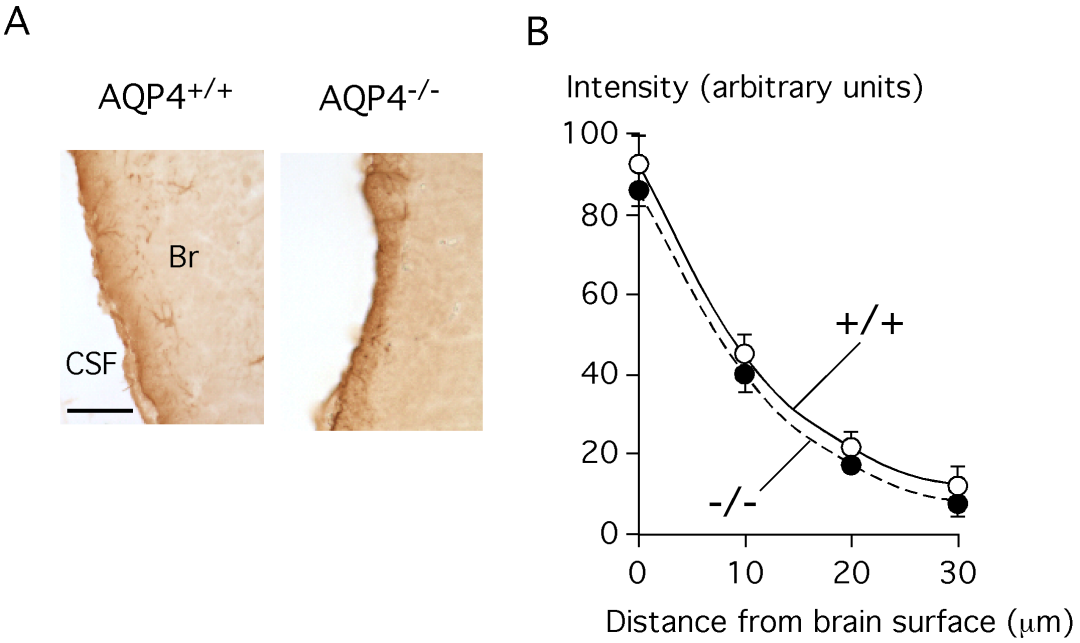

Figure 17. GFAP expression – glia limitans. A. GFAP immunostaining (brown) of the glia limitans externa in 2 +/+ *vs.* 2 -/- mice. CSF – cerebrospinal fluid, Br – brain parenchyma **B.** Plots of GFAP staining intensity *vs.* distance from the brain surface from 5 +/+ and 5 -/- mice (mean ± SEM). The differences between +/+ and -/- are not significant. Bar = 40 μm (**A**).

[Adapted from Saadoun S, Tait MJ *et al.* AQP4 gene deletion in mice does not alter blood-brain barrier integrity or brain morphology. *Neuroscience.* 2009 Jul 7;161(3):764-72.]

7.3 Structure and function of the BBB

I was particularly keen to confirm normal BBB integrity in AQP4 -/- mice. An open BBB would predispose the mice to vasogenic oedema making them unsuitable for experiments to study cerebral oedema. I assessed the structure of the BBB using electron microscopy (7.4.1) and the BBB integrity using HRP (7.4.2).

7.3.1 Ultrastructure of the BBB

Zhou *et al.* have reported profound visible ultrastructural defects on electron microscopy including swollen astrocyte foot processes (c.30%), perivascular vacuoles and open endothelial tight junctions (>30%) (Zhao et al. 2005). These changes are associated with pathological opening of the BBB and if present would demonstrate BBB dysfunction.

I studied 20 sections from the cerebral cortex and caudate nucleus of 3 wildtype mice and 20 sections from the cerebral cortex and caudate nucleus of 3 AQP4 wildtype mice with representative photomicrographs shown in **Figure 19 A&B**. I chose examples of both superficial and deep grey matter for the test due to the high density of both capillaries and astrocytes present for study.

The ultrastructure of cortical and caudate nucleus microvessels in my AQP4 -/- mice appeared normal with endothelial cells joined by tight junctions and surrounded by astrocyte foot processes. I examined 60 microvessels from the cerebral cortex and the 60 from the caudate nucleus of the 3 wildtype and 3 AQP4 -/- mice and did not detect any astrocyte foot process swelling **(Figure 18 A-D)**. The lack of astrocyte foot

process swelling in our AQP4 -/- mice made it impossible for me to measure the perimicrovessel edema on the electron micrographs. For comparison, I show in **Figure 18G** a microvessel with marked surrounding astrocyte foot process edema taken from the forebrain of an AQP4 -/- mouse with streptococcal meningitis. All tight junctions from the 3 AQP4 -/- mice (15 in cerebral cortex and 15in caudate nucleus) appeared normal and, when considering serial sections, the tight junctions extended from the microvessel lumen to the endothelial basement membrane with no discontinuities **(Figure 18 E&F)**

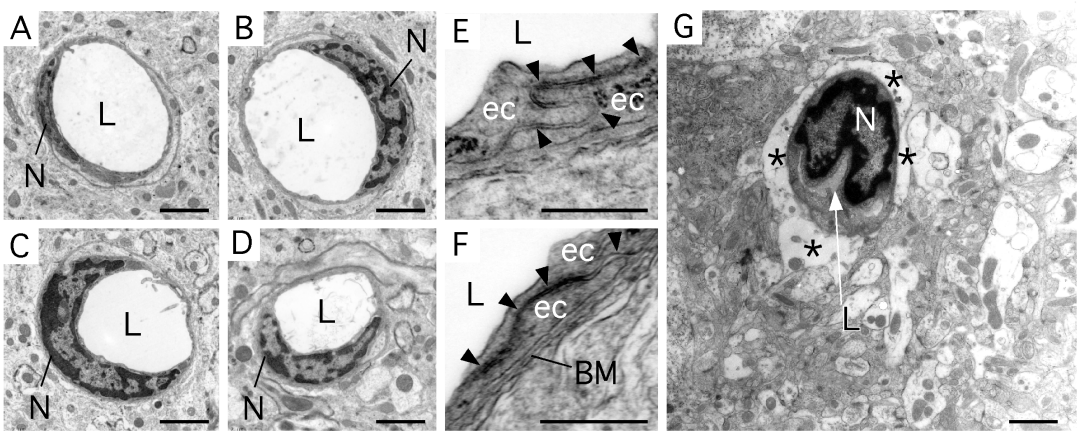

Figure 18. Blood-brain barrier – electron micrographs. A-D. Four capillaries from -/- mouse cerebral cortex showing the lumen (L) and endothelial cell nucleus (N) surrounded by intact astrocyte foot processes. **E, F.** Two tight junctions (arrowheads) from -/- mouse cerebral cortex located between adjacent endothelial cells (ec) and extend from the capillary lumen (L) to the endothelial basement membrane (BM). **G.** Capillary 48 h after streptococcal meningitis showing endothelial cell nucleus (N), astrocytic foot process swelling (*) and collapsed capillary lumen (L). Bars 2 μm (**A-D**, **G**), 0.5 μm (**E**, **F**). [Adapted from Saadoun S, Tait MJ *et al.* AQP4 gene deletion in mice does not alter blood-brain barrier integrity or brain morphology. *Neuroscience.* 2009 Jul 7;161(3):764-72.]

7.3.2 Functional assessment of the BBB

Experimental assessment of the BBB is done by injecting a large molecule into the blood and then examining the brain histologically to see whether any has entered the brain extracellular space. As an intact BBB will prevent such molecules from entering the brain their presence demonstrates BBB dysfunction. Several such molecules can be used including labeled dextrans, Evans blue and HRP. Zhou *et al* add weight to their findings of BBB structural abnormalities by demonstrating extravasation of HRP in AQP4 -/- mice (Zhao et al. 2005). I therefore chose to assess BBB function using HRP to provide a direct comparison with Zhou *et al*'s findings. HRP is a 45kDa molecule that if injected intravenously will not cross an intact BBB. It has a molecular diameter of 600nm, very similar to that of albumin (c.750nm), and so is a good marker of increased BBB protein permeability (Vorbrodt and Dobrogowska 2003).

The BBB in wildtype and AQP4 -/- mice was impermeable to intravascular HRP in all brain sections examined. In the one AQP4 -/- mouse subjected to focal cortical freeze injury, marked extravasation of HRP was observed from microvessels at the site of the injury, into the surrounding brain parenchyma (Fig. 5J and inset).

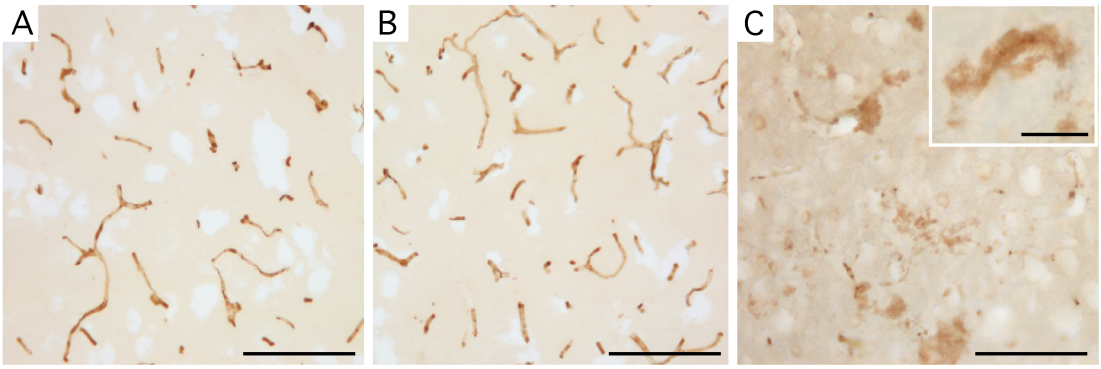

Figure 19. Blood brain barrier – horseradish peroxidase injection. Cerebral cortex from **A.** an intact +/+ mouse, **B.** an intact -/- mouse, and **C.** a +/+ mouse after cortical freeze injury. HRP was injected intravenously and was visualized brown by DAB staining. Magnified view of leaky microvessel (*inset*). 'Holes' in the tissue are a processing artifact. Bars 100 μm (A-C), 10 μm (C inset).

[Adapted from Saadoun S, Tait MJ *et al.* AQP4 gene deletion in mice does not alter blood-brain barrier integrity or brain morphology. *Neuroscience.* 2009 Jul 7;161(3):764-72.]

8.1 Design of a mouse model for the study of cerebral oedema after SAH

Having shown no major baseline abnormalities between AQP4 -/- and wildtype mice, I investigated the role of AQP4 in brain oedema. Given the uncertainty surrounding the mechanism of cerebral oedema formation following SAH it was important that my experimental model needed to fulfill strict criteria. First, both the volume of subarachnoid blood and the resulting pressure rise had to be reproducible. Secondly, the experimental SAH had to consistently produce oedema without an unacceptably high mortality rate. Finally, the technique should, ideally, be straightforward and quick to perform.

Pre-existing rodent models of SAH generally require either direct injection of blood into the foramen magnum or endovascular perforation of the circle of Willis. To inject blood into the cisterna magna the posterior atlanto-occipital membrane is exposed and perforated with a fine bore needle (Lin et al. 2003; Solomon et al. 1985). This membrane is fragile so to avoid loss of injected blood by back-bleeding a slow injection is used which prevents a reproducible rise in ICP to levels seen in SAH. A further flaw with this technique is that blood is delivered to the posterior basal cisterns whereas >90% of aneurysms arise in the anterior circulation (Kassell et al. 1990).

For the perforation model a sharpened monofilament suture is inserted into the internal carotid artery and advanced rostrally as far as the anterior cerebral artery and middle cerebral artery bifurcation. The suture is then pushed through the vessel wall causing SAH (Bederson et al. 1995; Veelken et al. 1995). This model mimics the

process of SAH well but does not allow control of either the volume or ICP rise of the resulting haemorrhage. In mice this technique is technically challenging and results in a 20-30% mortality rate at 72 hours (Kamii et al. 1999; Saito et al. 2001).

To overcome these problems I modified a technique of direct injection of blood into the basal cisterns previously described in rats (Prunell et al. 2002) (described in 6.11). To confirm that my technique injected blood into the subarachnoid space I exposed the dura overlying the cerebellum and the thoracic spinal cord. I then performed the injection and was able to see directly the spread of blood within the CSF space **(Figure 20)**.

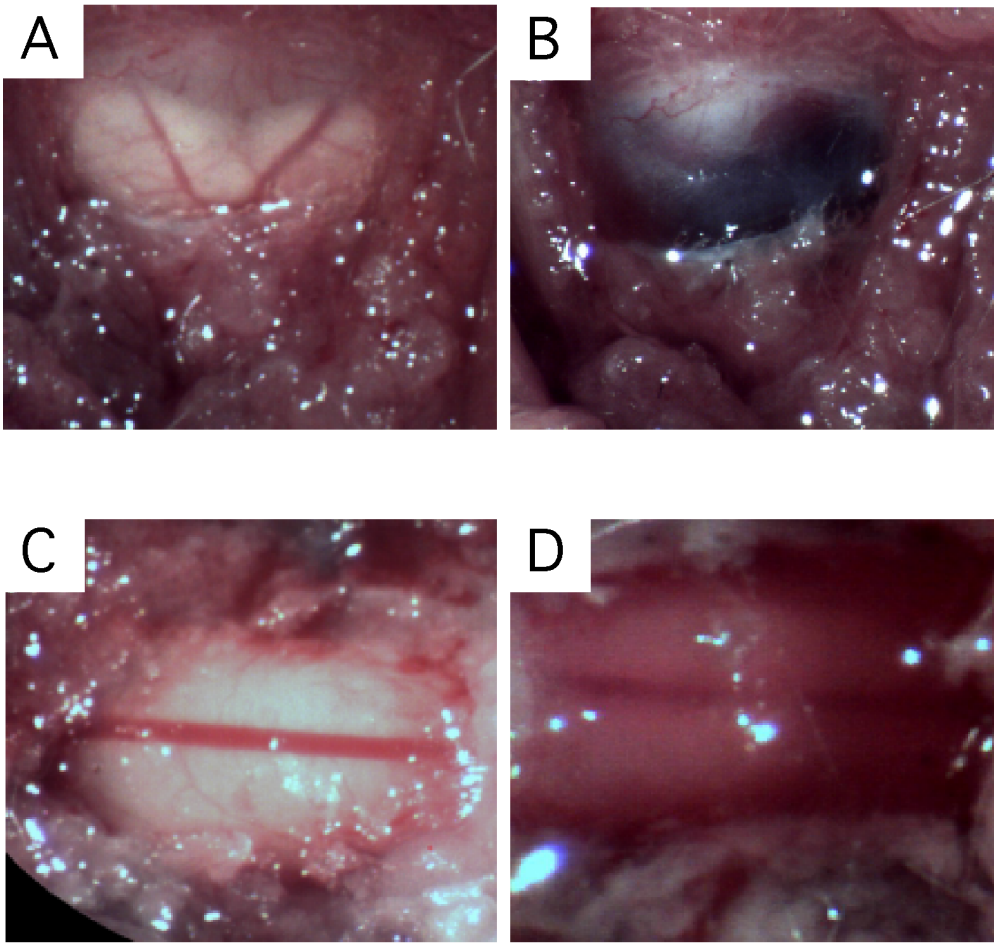

Figure 20. Confirmation that injection is into the subarachnoid space. Exposed dura overlying cisterna magna **(A)** and spinal cord **(B)** at T6. After injecting blood into the basal cisterns haemorrhage can clearly be seen within the subarachnoid space at both sites **(C&D)**.

[Adapted from Tait MJ *et al.* Increased brain oedema after subarachnoid hemorrhage in *aqp4*-null mice. *Neuroscience.* 2010 Apr 28;167(1):60-7.]

Using a syringe driver I was able to perform injections with consistently reproducible pressure profiles. I was able to vary both the volume and the rate of the injection. Increasing either parameter led to an increase in the maximum injection ICP. To mimic SAH I aimed for a maximum ICP similar to known murine systolic blood pressure. As cerebral oedema after SAH is associated with more severe haemorrhages in humans I balanced the injection volume and rate to give as large a volume as possible without giving an unacceptable mortality rate but still giving the injection over a short period to simulate an acute event.

Once the parameters were set I was able to give injections of a precise volume with a highly reproducible pressure profile. As soon as the injection was completed the ICP immediately began to fall but to a plateau greater than before the injection **(Figure 21)**

To demonstrate that cerebral oedema was due to the SAH rather than another aspect of the procedure such as brain trauma or hypoxia during anaesthesia I used a sham needle insertion with no injection as a control. Injection of saline instead of blood is not a suitable control as it will lead to a rise in ICP and may therefore generate oedema. Following sham needle insertion there was no elevation in either ICP or brain water content at 6 or 24 hours **(Figures 25 & 26)** and little change in the neurological score at either time point **(Figure 24).**

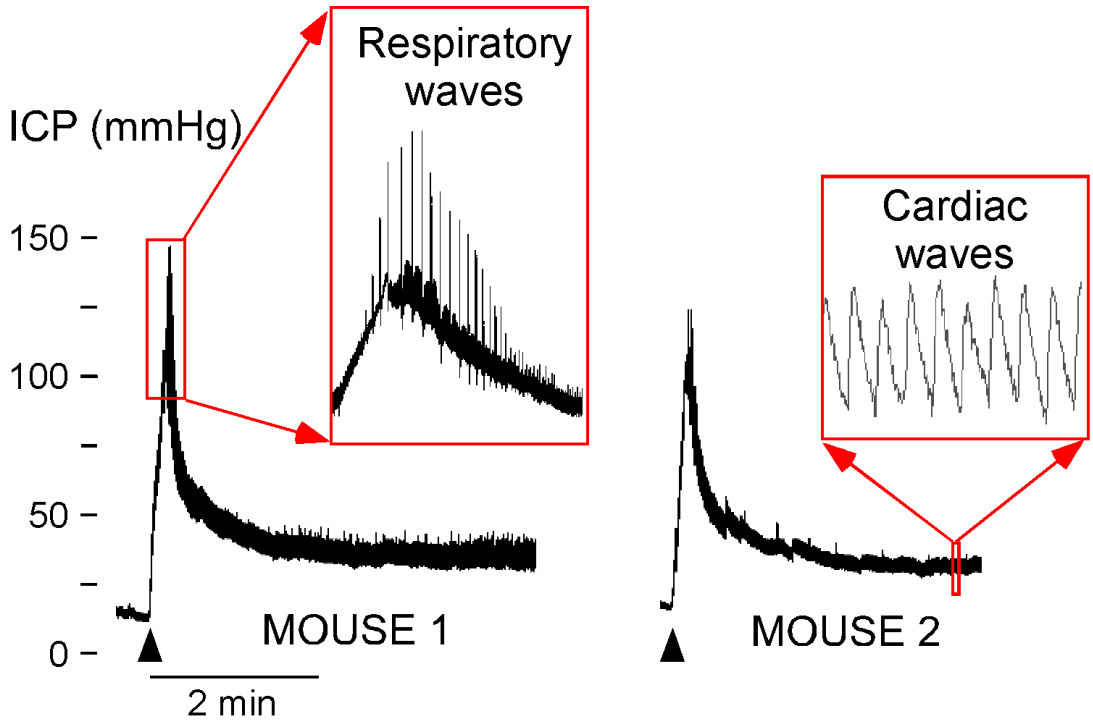

Figure 21. Typical ICP traces. Arrowheads show onset of blood injection. Inset 1: prominent respiratory waves: mice became apnoeic at high ICP. Intermittent gasps were associated with spikes of increased ICP. This settled spontaneously as ICP fell. Inset 2: cardiac ICP pulsations.

[Adapted from Tait MJ *et al.* Increased brain oedema after subarachnoid hemorrhage in *aqp4*-null mice. *Neuroscience.* 2010 Apr 28;167(1):60-7.]

8.2 Exclusion of hydrocephalus

Hydrocephalus is a well-recognized complication of SAH, occurring acutely in 21% of cases (Milhorat 1987). The development of hydrocephalus in the model would make results harder to interpret. Enlarged ventricles will increase intracranial pressure and whole brain water content as well as most likely altering the neurological score. Hydrocephalus is known to progress faster in AQP4 -/- mice (Bloch et al. 2006b).

I compared the 3rd ventricular size after SAH and sham injection in both wildtype and AQP4 -/- mice and found no cases of hydrocephalus. This strongly implies that the model does not produce hydrocephalus. The direction of the SAH 'jet' was inferior, towards the skull base. This is often not the case in aneurismal SAH: aneurysms may point toward the ventricles causing intraventricular haemorrhage on rupture and subsequent hydrocephalus.

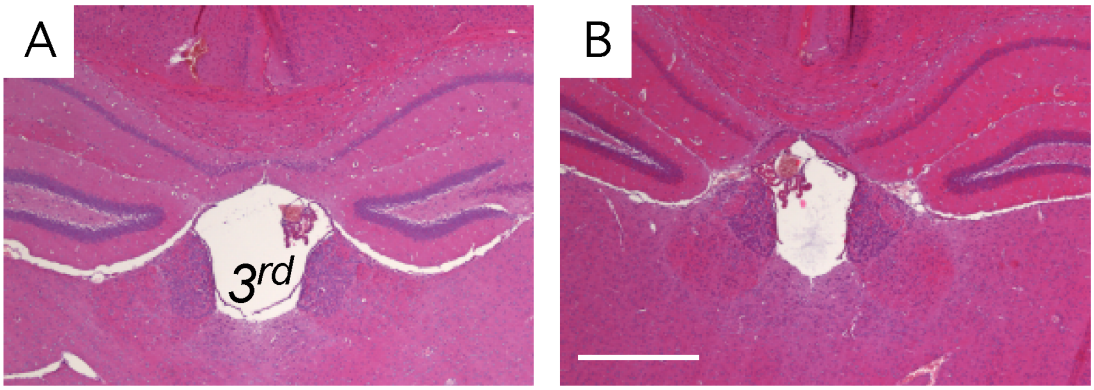

Figure 22. Histological examination for hydrocephalus. Coronal brain section at 2.8 mm from the frontal poles stained with hematoxylin-eosin showing normal-sized 3rd ventricle 24 h after sham injection or SAH. Bar = 0.5 mm.

[Adapted from Tait MJ *et al.* Increased brain oedema after subarachnoid hemorrhage in *aqp4*-null mice. *Neuroscience.* 2010 Apr 28;167(1):60-7.]

8.3 Classification of oedema produced by the model.

Once it was clear that the model consistently produced cerebral oedema following SAH I tried to characterize the type of oedema produced. The fundamental difference between cytotoxic and vasogenic oedema is the condition of the BBB. Any molecule seen within the brain parenchyma must have passed through the BBB. By injecting different sizes of albumen bound to different fluorescent molecules into the vasculature I aimed to see what size of molecule, if any, would pass through the BBB. Very large 2MDa dextran molecules bound to FITC would not be expected to pass through even an open BBB. Smaller 10kDa dextrans bound to rhodamine should pass into the brain parenchyma if the BBB is open but not if it is closed. As the two molecules attached to the dextrans fluoresce different colours at different frequencies it is possible to study the position of the molecules simultaneously at the same capillary. I injected the dyes into two wildtype mice 6 hours after SAH and two wildtype mice 6 hours after just needle insertion as a control.

I found that in both controls and SAH mice the 2MDa FITC-dextran remained within the capillaries. The 10kDa rhodamine-dextran remained within the capillaries of the control mice but extravasated in the SAH mice **(Figure 23)**. This demonstrates that the BBB is damaged by the SAH in my model and that the cerebral oedema produced is vasogenic. I subsequently confirmed this finding using Evans blue dye (see below – **Figure 27).**

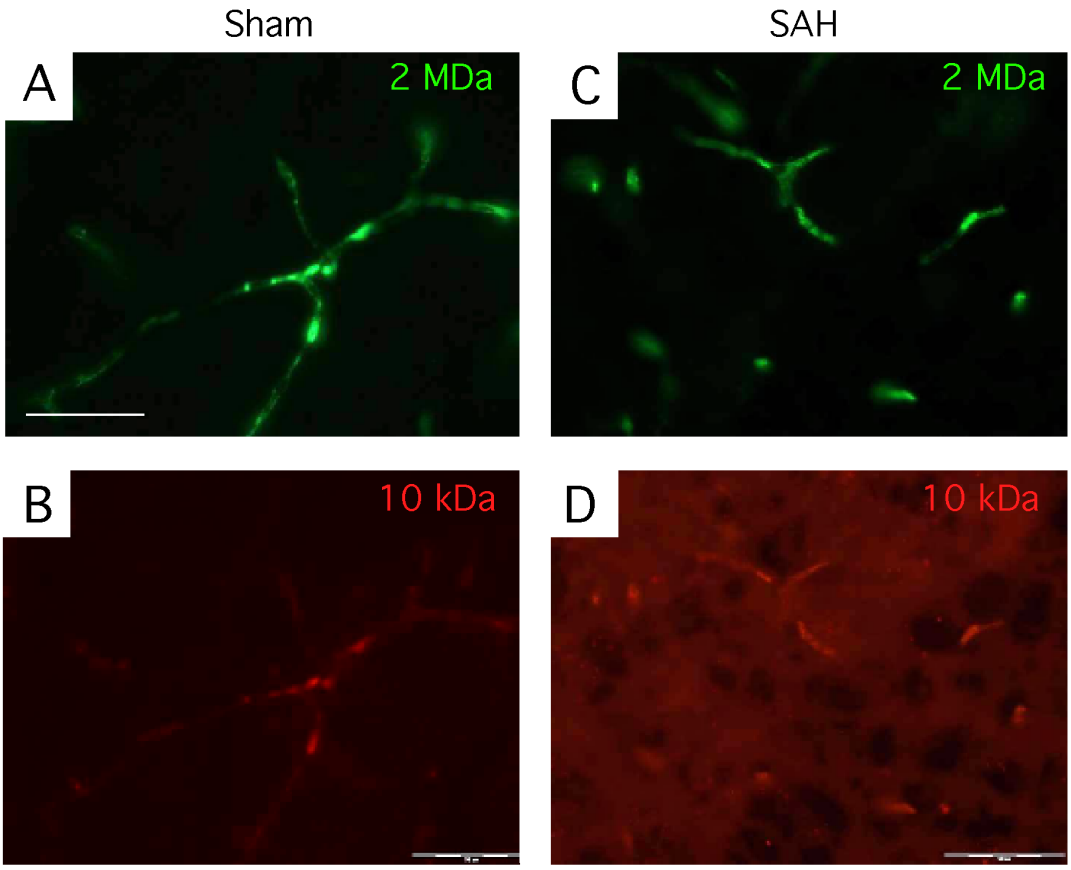

Figure 23. Demonstration of BBB damage following SAH. A and B. Brain sections 24h after sham needle insertion (Sham) showing no extravasation of either size dextran. **C and D.** Brain sections 24 h after SAH. There is extravasation of the smaller dextran only. Mice had *i.v.* injection of 10 kDa rhodamine-dextran (red) and 2 MDa FITC-dextran (green). Bar = 50 μm.

[Adapted from Tait MJ *et al.* Increased brain oedema after subarachnoid hemorrhage in *aqp4*-null mice. *Neuroscience.* 2010 Apr 28;167(1):60-7.]

8.4 Assessment of cerebral oedema after SAH.

Three methods were used to look for a difference in cerebral oedema in the two groups. Cerebral oedema is defined as an increase in brain water content producing an increase in brain volume. Brain water content was measured directly using the dry/ wet mass method. The relationship between brain volume and intracranial pressure (described by the Monro-Kellie principle) allowed the measurement of ICP as an indirect reflection of brain volume. As the brain is contained within the rigid cranial vault an increase in brain volume will lead to an increase in intracranial pressure. Although the relationship between pressure and volume is not linear (described by the Monro-Kellie curve) it does allow comparison between the two groups. The third measurement of cerebral oedema was a neurological examination. In order to be clinically relevant, cerebral oedema should result in objective changes in behaviour.

I used all three methods of assessment in each mouse. At the appropriate time point a neurological assessment was performed. The mouse was then anaesthetized and the ICP recorded. Immediately afterwards the mouse was sacrificed and the brain was removed to perform the dry/ wet measurement of brain water content. To prove that the results were not time dependent the experiment was performed twice using two different time points.

The neurological score was significantly better in the wildtype mice at both 6 and 24 hours **(Figure 24)**. Both intracranial pressure and brain water content were

significantly higher in AQP4 -/- mice **(Figures 25 &26).** Taken together these data shows that cerebral oedema is greater in the AQP4 -/- mouse at both 6 and 24 hours.

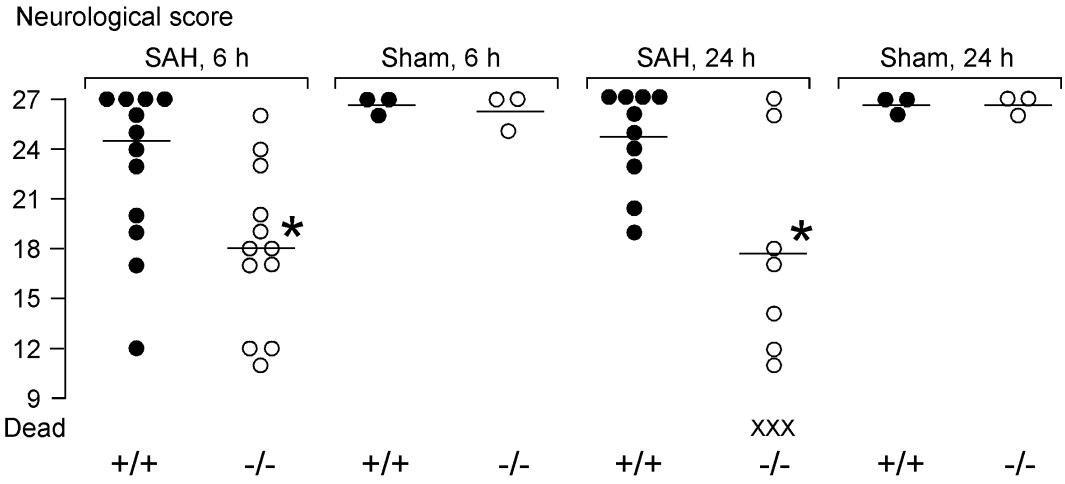

Figure 24. Neurological scores after SAH. Neurological score at 6 and 24 h after saline injection or SAH in wildtype and AQP4 -/- mice. Data from sham needle insertions are provided as controls. ● = Wildtype (+/+),○ = AQP4 -/- (-/-), X = dead mice. — = median. **P* < 0.05 for wildtype *vs.* AQP4 -/-.

[Adapted from Tait MJ *et al.* Increased brain oedema after subarachnoid hemorrhage in *aqp4*-null mice. *Neuroscience.* 2010 Apr 28;167(1):60-7.]

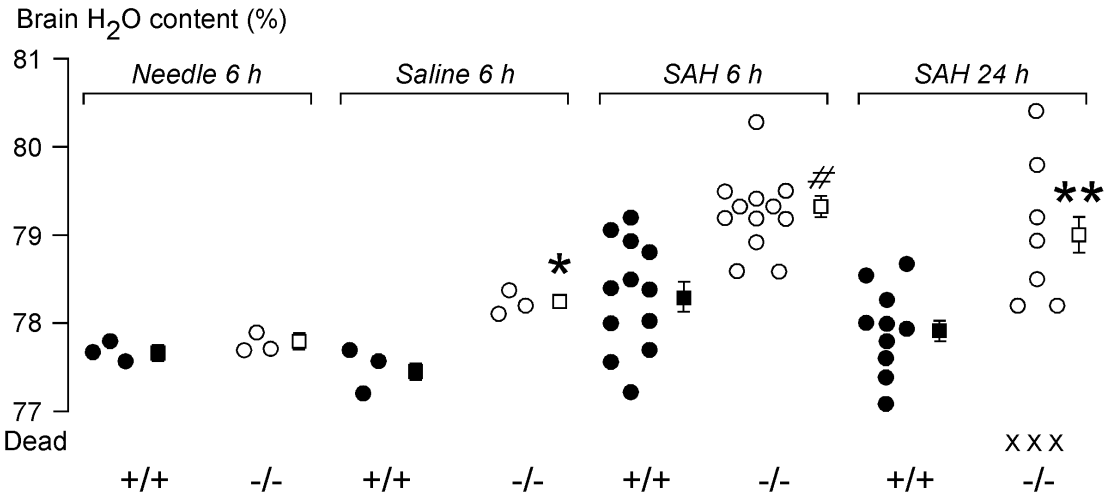

Figure 25. Brain water content after SAH. **A.** Whole brain water content measured at 6 and 24 h after needle insertion, saline injection, or SAH. Data from needle insertion shams for control. Brain water content after saline injection was greater in the AQP4 -/- mice but not as great as after SAH. ● = Wildtype (+/+), ○ = AQP4 -/- (-/-), X = dead mice. ■ = Mean of wildtype, □ = Mean of AQP4 -/-, Error lines = ±SEM. *$P < 0.05$, **$P < 0.01$, #$P < 0.0005$ for wildtype *vs*. AQP4 -/-.

[Adapted from Tait MJ *et al.* Increased brain oedema after subarachnoid hemorrhage in *aqp4*-null mice. *Neuroscience.* 2010 Apr 28;167(1):60-7.]

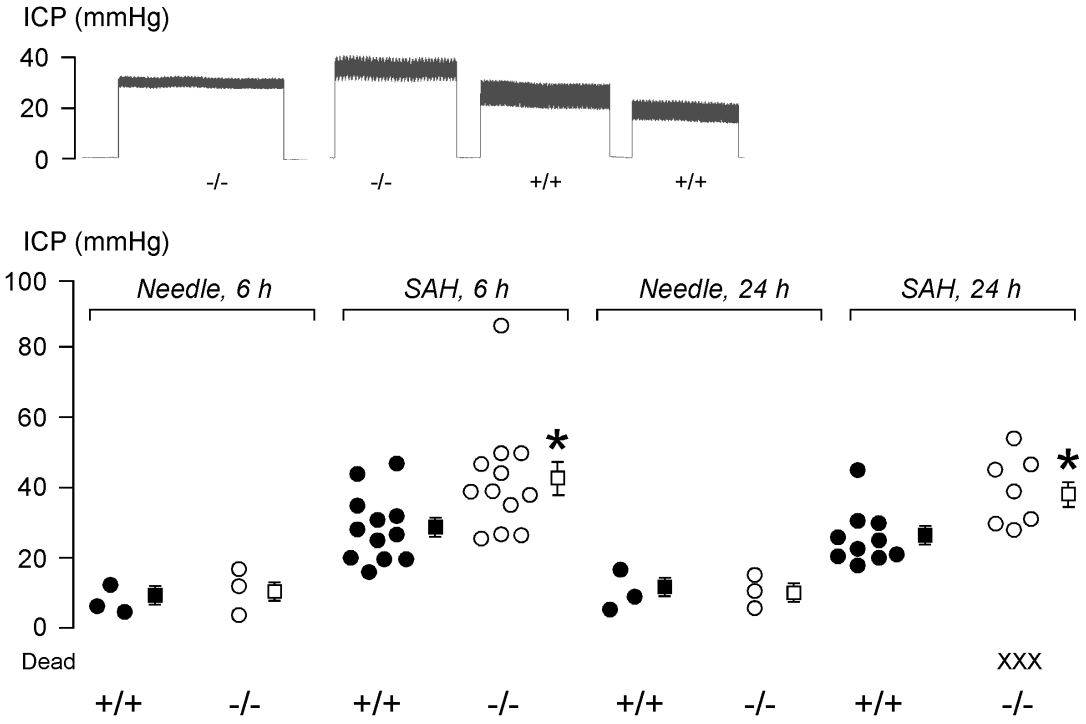

Figure 26. Intracranial pressure after SAH. (Top) Typical ICP recordings from 2 wildtype and 2 AQP4 -/- mice at 6 h after SAH and (Bottom) summary of ICP data measured at 6 and 24 h after needle insertion or SAH with needle insertion sham controls.

● = Wildtype (+/+), ○ = AQP4 -/- (-/-), X = dead mice. ■ = Mean of wildtype, □ = Mean of AQP4 -/-, Error lines = ±SEM. *$P < 0.05$ for wildtype *vs*. AQP4 -/-.

[Adapted from Tait MJ *et al.* Increased brain oedema after subarachnoid hemorrhage in *aqp4*-null mice. *Neuroscience.* 2010 Apr 28;167(1):60-7.]

8.5 Mechanism of formation of cerebral oedema

I also tried to identify whether the ICP rise of the SAH or the presence of the blood in the basal cisterns contributed more to the formation of oedema. Injection of the same volume of saline at the same rate as the SAH led to an increase in brain water content at 6hours but the rise was not as great as with SAH **(Figure 25)**. Saline injections did not lead to as high rises in ICP as blood injections. This may be due to the lower viscosity of the saline, which would allow it to escape more easily into the spinal canal. The lower brain water content in the saline injected mouse may therefore be due to the lower peak injection pressure or due to a direct effect of the blood within the cisterns.

As I had previously demonstrated that the oedema is due to opening of the BBB **(Figure 23)**. I wanted to see if the difference in oedema formation between the two groups was due to a difference in the degree of BBB opening. Evans blue dye is a small molecule that binds to albumen when injected intravenously. It will only enter the brain if the BBB is damaged. By leaving the brain overnight in a known volume of formamide it is possible to extract the Evans blue that has crossed the BBB. The concentration of Evans blue can then measured using the absorbance spectrum of the formamide/ Evans blue. I found that more Evans blue leaked into the brain after SAH than after needle insertion sham controls confirming the previous finding that the BBB was open. There was no difference in the degree of BBB opening between the wildtype and AQP4 -/- mice indicating that the extent and mechanism of oedema *formation* is similar in both groups **(Figure 27).** This would be expected for

vasogenic oedema as once the BBB is open excess fluid enters the brain by an AQP4 independent pathway.

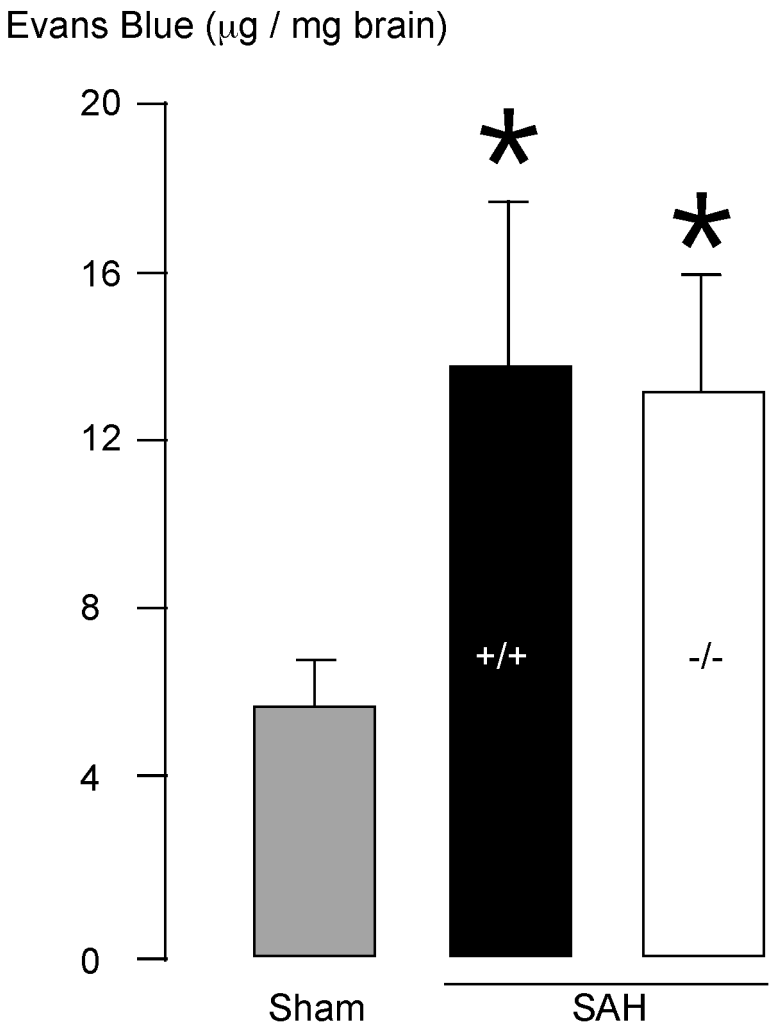

Figure 27. Summary of Evans blue data. N = 4 (Sham, 2 +/+ and 2 -/-), 3 (SAH, +/+), 3 (SAH, -/-). Mean ± SEM. *$P < 0.05$ compared with needle insertion sham. [Adapted from Tait MJ *et al.* Increased brain oedema after subarachnoid hemorrhage in *aqp4*-null mice. *Neuroscience.* 2010 Apr 28;167(1):60-7.]

8.6 Mechanism of resolution of cerebral oedema.

If oedema formation is via the same APQ4 independent pathway in the two mice then the differences in the ICP, brain water content and neurological score must be due to a difference in the rate of oedema elimination. It has previously been suggested that oedema clearance into the CSF via either the pia mater or the ependyma is AQP4 mediated and that AQP4 -/- mice are therefore less effective at clearing excess fluid and so more prone to vasogenic oedema.

There have been no experiments to date that demonstrate a reduction in the permeability of the glia limitans to water in AQP4 -/- mice. Measuring the water flow across the glia limitans is technically challenging due to the highly specific nature of the water channel: any form of dye or marker will not pass through the AQP4 and so will not allow comparison. A second problem encountered *in vivo* is that any water leaving the brain will immediately be absorbed into the much larger volume of CSF.

To avoid these two problems I decided to take advantage of the bidirectional nature of AQP4 channels. I set up an osmotic gradient into the brain by placing a hypotonic agarose block against the brain convexity. The amount of water crossing into the brain in a given time will be dependent on the permeability of the glia limitans to water. The brain water content of the cerebral hemisphere applied to the agarose block was measured and compared to the other hemisphere (which had not been exposed to the osmotic gradient) to assess the *increase* in brain water content. I used isotonic agarose blocks as a control for other causes of oedema formation, particularly brain trauma during the craniectomy.

I found that the difference between hemispheres was greater in wildtype than AQP4 -/- mice showing that more water had entered and that the glia limitans is less permeable in the AQP4 -/- mice **(Figure 28)**.

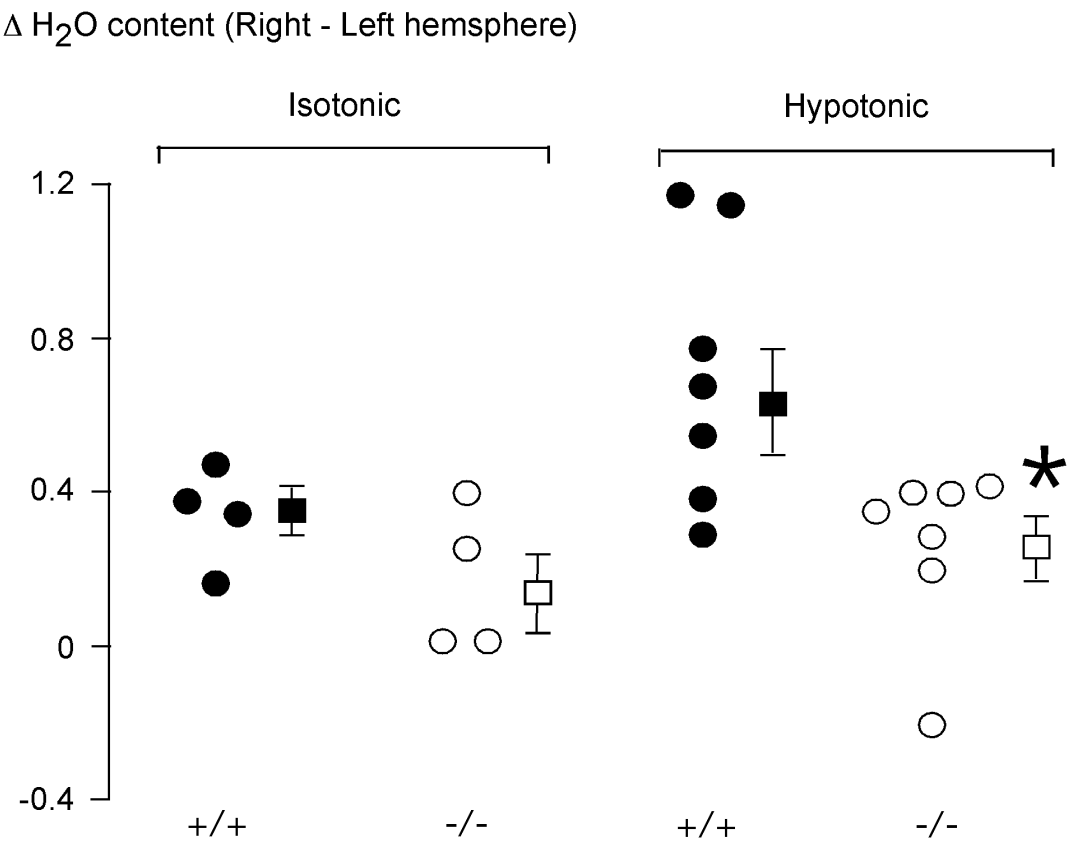

Figure 28. Permeability of the glia limitans to water. Difference in % water content between right and left hemispheres (DH_2O) in wildtype (●, +/+) and KO (○, -/-) mice exposed to 4 % agarose gel in water (hypotonic) or 0.9 % saline (isotonic). ■ = Mean of wildtype, □ = Mean of KO, Error lines = ±SEM. **P* < 0.02.

[Adapted from Tait MJ *et al.* Increased brain oedema after subarachnoid hemorrhage in *aqp4*-null mice. *Neuroscience.* 2010 Apr 28;167(1):60-7.]

8.7 Changes in AQP4 expression after experimental SAH.

As oedema clearance following SAH is dependant on AQP4 I wanted to see if SAH led to increased expression of AQP4 at the glia limitans in wildtype mice. This would be an appropriate adaptive response to increase the rate of oedema clearance.

I found that following SAH that there was remarkable upregulation of AQP4 protein in wildtype mice at both the glia limitans and the pericapillary regions when compared to mice after sham needle insertion. In control experiments, no aqp4 immunoreactivity was detected in KO mice or when the primary antibody was omitted **(Figure 29).**

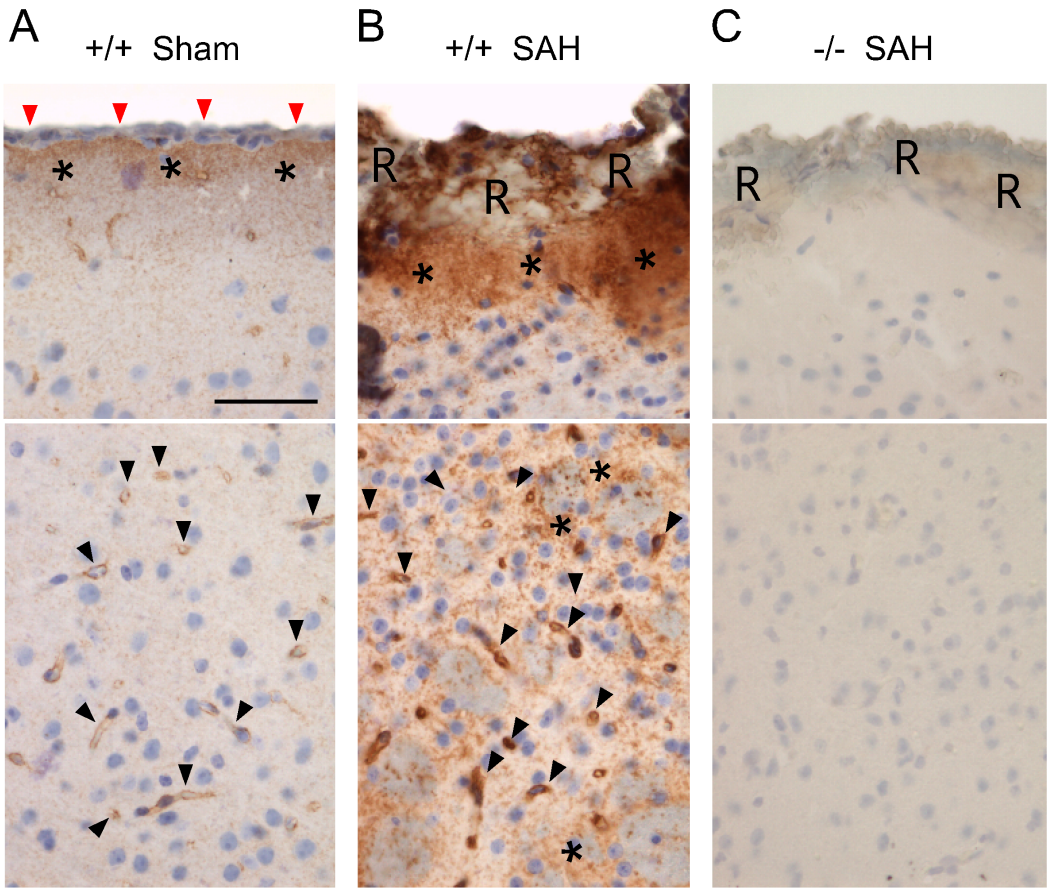

Figure 29. AQP4 immunoreactivity after SAH. (top) Glia limitans. (bottom) Brain parenchyma. **A.** Sham wildtype mouse. Red arrows indicate the pia and asterisks the glia limitans. Arrowheads show microvessels. **B.** Wildtype mouse 24 h after SAH. 'R' indicates red blood cells overlying the pia and asterisks the sub-pial region. Arrowheads show microvessels and asterisks show AQP4 immunoreactivity in the brain parenchyma. **C.** AQP -/- mouse 24 h after SAH. 'R' indicates red blood cells covering the pia. Bar = 50 µm.

Discussion

9.1 Baseline comparison of AQP4 -/- and wildtype mice

On the basis of my findings I conclude that AQP4 deletion in mice does not produce any baseline abnormalities in cortical neuronal and non-neuronal cell densities, GFAP expression, white matter myelination, microvessel endothelial cell morphology, or BBB permeability.

Accurate brain water homeostasis requires careful balance of the flow of water into and out of the brain parenchyma as well as resistance to flow through the brain. The process therefore requires BBB integrity, normal parenchymal cell distribution and normal glia limitans structure.

To assess BBB integrity I examined both the morphology and function of the BBB. Similar expression of GFAP around capillaries in both wildtype and AQP4 -/- mice indicates that the density of astrocyte foot processes at the BBB is unaltered in the AQP4 -/- mouse. At the ultrastructural level, integrity of the endothelial tight junctions, which is a prerequisite for BBB function was readily apparent. Electron microscopy also failed to show evidence of astrocyte foot process swelling, a hallmark of BBB dysfunction. I assessed the physiological function of the AQP4 -/- mouse BBB using the horseradish peroxidase extravasation test. I was unable to identify any horseradish peroxidase within the brain parenchyma indicating that the BBB is impermeable to larger molecules in the AQP4 -/- mouse. Taken together

these results confirm BBB competence under physiological conditions despite AQP4 gene deletion.

I also evaluated the cellular architecture of both the white and grey matter of the AQP4 -/- brain parenchyma. I found no difference in either white matter tract size or the extent of tract myelination indicating normal development. On analysis of the grey matter the cellular density of both neurons and astrocytes was unaltered in the AQP4 -/- mice. The microstructure of the glia limitans was also found to be unchanged in the AQP4 -/- mouse. These findings show no potential for abnormalities of either parenchymal resistance to water flow or of fluid clearance via the glia limitans.

Several baseline characteristics of the AQP4 -/- mice used in my experiments have been assessed in the course of previous experiments. Previously published data comparing AQP4 -/- mice with wildtype mice also do not reveal any differences in anatomical or physiological parameters (arterial blood pressure, intracranial pressure, bulk intracranial compliance), blood chemistries or BBB integrity (Table 1). Previous ultrastructural studies of the perimicrovessel astrocyte foot process in the brains of AQP4 -/- mice showed them to be indistinguishable from those in wildtype mice (Manley et al. 2000; Papadopoulos and Verkman 2005). Functional studies, using the Evans Blue extravasation technique (Bloch et al. 2005; Feng et al. 2008; Papadopoulos et al. 2004), also demonstrated normal BBB permeability after AQP4 deletion.

One potential explanation for the lack of baseline differences between the two groups is that AQP4 deletion could produce compensatory upregulation of other AQPs in the brain. This has previously been investigated and shown not to be the case: expression of both AQP1 and AQP9 are unchanged in AQP4 -/- mice (Papadopoulos et al. 2004). The only established difference in brain phenotype in AQP4 -/- mice is an expanded extracellular space compared to wildtype mice (Binder et al. 2004; Yao et al. 2008; Zador et al. 2008).

At each stage of brain water homeostasis I was unable to identify any significant difference in structure or function between AQP4 -/- and wildtype mice. My data therefore validate the AQP4 -/- mouse as an excellent research subject for investigation into cerebral oedema.

9.2 Potential explanation of conflicting findings in the Nanjing AQP4 -/- mouse.

Recently Zhou et al reported marked abnormal baseline characteristics in an independently generated AQP4 -/- mouse including markedly reduced GFAP expression, increased BBB permeability, and tight junction abnormalities (Zhou et al. 2008). The BBB disruption described in the Nanjing AQP4 -/- mice is severe. They report that the BBB in AQP4 -/- mice is freely permeable to large molecules such as HRP (MW 44 kDa) and that >30 % of brain endothelial tight junctions are open, with a marked increase in perimicrovessel astrocyte foot process area. The amount of BBB opening described is comparable to that seen after severe brain injury. It is, therefore, surprising that the Nanjing AQP4 -/- mice are viable. Such a degree of

brain abnormality, if present throughout the brain, would be expected to be incompatible with life.

Zhou *et al*.'s (2008) reported marked BBB disruption might be explained by artifacts produced by perfusion-fixation. Forceful perfusion of fixative through the left cardiac ventricle, mechanical damage to the brain during extraction or hypoxic brain injury produced by terminal anaesthesia may produce perimicrovessel astrocyte foot process oedema. Tight junctions are tortuous structures and therefore tight junction discontinuities may represent tissue-sectioning artifacts and need to be confirmed by examining serial tissue sections. GFAP expression around individual vessels is highly variable and therefore differences in GFAP immunoreactivity could easily represent a selection bias. It is also possible that the Nanjing AQP4 -/- mice have various (non-AQP4) genetic abnormalities that were produced during the genetic targeting process.

Recently the Nanjing group have reported subfertility in their female AQP4 -/- mice (X. L. Sun et al. 2008). Subfertility has not been observed in San Francisco AQP4 -/- mice that are now being bred by several groups including A.S. Verkman and G.T. Manley in San Francisco, D. Binder in Irvine, and M.C. Papadopoulos in London. At St. George's, 29 AQP4 -/- × AQP4 -/- *vs.* 23 wildtype × wildtype matings of CD1 mice produced litter sizes of 9.3 ± 0.5 (mean ± SEM) *vs.* 10.5 ± 0.6 mice and male: female ratios of 0.9:1 *vs.* 1.2:1 mice, respectively. These data suggest that AQP4 deletion does not produce major fertility problems in mice.

9.3 The role of AQP4 in the pathophysiology of SAH induced cerebral oedema

The principal finding of the SAH studies is that AQP4 -/- mice develop more brain oedema after SAH than wildtype mice. AQP4 -/- mice had higher ICP, increased brain water content and lower neurological scores than wildtype mice at 6 and 24 h after SAH. I propose that SAH causes equal vasogenic oedema in both AQP4-/- and wildtype mice via an AQP4 independent disruption of the BBB. Faster elimination of excess water via AQP4 in wildtype mice then results in greater oedema in the AQP4 -/- mice.

9.4 Novel model of SAH

My conclusions are based on a new SAH model. Previous rodent SAH models include endovascular perforation of the basilar (Barry et al. 1979) or internal carotid arteries (Veelken et al. 1995), or cisterna magna injection of autologous blood (Solomon et al. 1985). Endovascular perforation does not allow control of injected blood volume or ICP. Cisterna magna injection does not deliver blood into the correct anatomical site (basal cisterns) and has the key problem of back-bleeding when high-pressure injections are attempted. Previous models therefore do not allow the induction of SAH with a predetermined pressure *and* volume.

I used a syringe driver to reproducibly inject blood into the basal cisterns at high pressure with no intraparenchymal haematoma formation. The brain around the needle prevented ‘back-bleeding’. This model allowed me to standardize both key parameters, injection pressure and injection volume. My SAH model does not

produce hydrocephalus or vasospasm during the first 24 h, but is associated with substantial brain oedema.

9.5 Formation and type of brain oedema in SAH

Brain oedema developed within 6 h of SAH may be caused in part by a direct chemical effect of blood in the CSF and in part by the sudden elevation in ICP. Several studies (Grote and Hassler 1988; Trojanowski 1984; Voldby and Enevoldsen 1982), have reported a sudden ICP rise during SAH, causing transient brain circulatory arrest. I propose that this abrupt increase in ICP damages the brain microcirculation causing a net flow of water into the brain *i.e.* vasogenic oedema. In agreement with this, MRI brain studies of SAH patients show a marked increase in the apparent diffusion coefficient, a characteristic of vasogenic oedema (Liu et al. 2007).

Experimentally induced SAH using my model resulted in vasogenic oedema; there was extravasation of intravascular macromolecules into the brain parenchyma, indicating increased BBB permeability after SAH. It is well-established that vasogenic cerebral oedema forms through an AQP4-independent route (Tait et al. 2008). Using Evans blue dye I found that BBB opening after SAH was comparable in wildtype and AQP4 -/- mice suggesting comparable production rates of vasogenic brain oedema.

9.6 Elimination of brain oedema in SAH

As the rate of cerebral oedema formation is similar in both AQP4 -/- and wildtype mice the difference in brain water content in the two groups must be related to a difference in fluid elimination.

The elimination of vasogenic brain oedema occurs through three AQP4-rich routes, the glia limitans, ependyma, and BBB (Tait et al. 2008). AQP4 -/- mice have reduced BBB osmotic permeability demonstrated by slowed brain swelling after acute water intoxication in AQP4 -/- *vs.* wildtype mice (Manley et al. 2000; Papadopoulos and Verkman 2005). Reduced water permeability of the ependyma in AQP4 -/- mice is demonstrated by slower water clearance from the ventricles into the brain in obstructive hydrocephalus in AQP4 -/- mice (Bloch et al. 2006b). Reduced osmotic permeability of the glia limitans in AQP4 -/- mice has not been demonstrated previously however I was able to do this using an agarose gel technique. Taken together, these findings suggest reduced oedema elimination in AQP4 -/- mice via all elimination routes – glia limitans, ependyma and capillaries.

9.7 AQP4 expression in SAH

AQP4 was upregulated in wildtype mice 24 h after SAH at key sites of oedema elimination including the glia limitans and pericapillary astrocyte processes. Increased AQP4 immunoreactivity has also been found in human brain after SAH (Badaut et al. 2003; Saadoun et al. 2003). I suggest that AQP4 upregulation is an adaptive response that increases the rate of oedema elimination after SAH.

Abbreviations

AQP	aquaporin
Ar/R	aromatic/ arginine
BBB	blood brain barrier
CD1	standard outbred mouse strain
CNS	central nervous system
CSF	cerebrospinal fluid
CT	computed tomography
DAB	diaminobenzidine
EBD	Evan's blue dye
ECS	extracellular space
GFAP	glial fibrillary acidic protein
HRP	horseradish peroxidase
ICP	intracranial pressure
ICS	intracellular space
MR	magnetic resonance
NPA	aspartine, proline, alanine
NeuN	neuronal nuclear marker
OCT	optimum cutting temperature
PBS	potassium buffered saline
SEM	standard error mean

Acknowledgements

I am indebted my two supervisors at St George's Dr Samira Saadoun and Mr Marios Papadopoulos as well as my supervisor at Oxford University, Mr Richard Kerr. I thank R. Moss and K. Szewczyk for help with electron microscopy.

I thank the Neurosciences Research Foundation and the Royal College of Surgeons of England Surgical Research Fellowship for supporting this research.

I performed the electron microscopy at St George's electron microscopy unit with help from Ceri Davies and Ray Moss.

Most of all I would like to thank Claire who was so patient while I was writing this!

References

Agre, P., et al. (2002), 'Aquaporin water channels--from atomic structure to clinical medicine', *J Physiol,* 542 (Pt 1), 3-16.

Amiry-Moghaddam, M., et al. (2005), 'Brain mitochondria contain aquaporin water channels: evidence for the expression of a short AQP9 isoform in the inner mitochondrial membrane', *Faseb J,* 19 (11), 1459-67.

Amiry-Moghaddam, M., et al. (2004), 'Alpha-syntrophin deletion removes the perivascular but not endothelial pool of aquaporin-4 at the blood-brain barrier and delays the development of brain edema in an experimental model of acute hyponatremia', *Faseb J,* 18 (3), 542-4.

Amiry-Moghaddam, M., et al. (2003), 'An alpha-syntrophin-dependent pool of AQP4 in astroglial end-feet confers bidirectional water flow between blood and brain', *Proc Natl Acad Sci U S A,* 100 (4), 2106-11.

Auguste, K. I., et al. (2007), 'Greatly impaired migration of implanted aquaporin-4-deficient astroglial cells in mouse brain toward a site of injury', *FASEB J,* 21 (1), 108-16.

Ayata, C. and Ropper, A. H. (2002), 'Ischaemic brain oedema', *J Clin Neurosci,* 9 (2), 113-24.

Badaut, J. and Regli, L. (2004), 'Distribution and possible roles of aquaporin 9 in the brain', *Neuroscience,* 129 (4), 971-81.

Badaut, J., et al. (2002), 'Aquaporins in brain: distribution, physiology, and pathophysiology', *J Cereb Blood Flow Metab,* 22 (4), 367-78.

Badaut, J., et al. (2003), 'Aquaporin 1 and aquaporin 4 expression in human brain after subarachnoid hemorrhage and in peritumoral tissue', *Acta Neurochir Suppl,* 86, 495-8.

Barry, K. J., Gogjian, M. A., and Stein, B. M. (1979), 'Small animal model for investigation of subarachnoid hemorrhage and cerebral vasospasm', *Stroke,* 10 (5), 538-41.

Bederson, J. B., Germano, I. M., and Guarino, L. (1995), 'Cortical blood flow and cerebral perfusion pressure in a new noncraniotomy model of subarachnoid hemorrhage in the rat', *Stroke,* 26 (6), 1086-91; discussion 91-2.

Binder, D. K., et al. (2004), 'In vivo measurement of brain extracellular space diffusion by cortical surface photobleaching', *J Neurosci,* 24 (37), 8049-56.

Binder, D. K., et al. (2006), 'Increased seizure duration and slowed potassium kinetics in mice lacking aquaporin-4 water channels', *Glia,* 53 (6), 631-6.

Bloch, O., Manley, G. T., and Verkman, A. S. (2006a), 'Accelerated progression of kaolin-induced hydrocephalus in aquaporin-4 deficient mice.', *J Cereb Blood Flow Metab*, In press.

Bloch, O., et al. (2005), 'Aquaporin-4 gene deletion in mice increases focal edema associated with staphylococcal brain abscess', *J Neurochem,* 95 (1), 254-62.

Bloch, O., et al. (2006b), 'Accelerated progression of kaolin-induced hydrocephalus in aquaporin-4-deficient mice', *J Cereb Blood Flow Metab,* 26 (12), 1527-37.

Brightman, M. W., Zis, K., and Anders, J. (1983), 'Morphology of cerebral endothelium and astrocytes as determinants of the neuronal microenvironment', *Acta Neuropathol Suppl,* 8, 21-33.

Brown, A. W. and Brierley, J. B. (1968), 'The nature, distribution and earliest stages of anoxic-ischaemic nerve cell damage in the rat brain as defined by the optical microscope', *Br J Exp Pathol,* 49 (2), 87-106.

Brown, P. D., et al. (2004), 'Molecular mechanisms of cerebrospinal fluid production', *Neuroscience,* 129 (4), 957-70.

Busch, E., et al. (1998), 'Diffusion MR imaging during acute subarachnoid hemorrhage in rats', *Stroke,* 29 (10), 2155-61.

Cahill, J., Calvert, J. W., and Zhang, J. H. (2006), 'Mechanisms of early brain injury after subarachnoid hemorrhage', *J Cereb Blood Flow Metab,* 26 (11), 1341-53.

Chen, C. H., et al. (2007), 'Effect of osmotherapy with hypertonic saline on regional cerebral edema following experimental stroke: a study utilizing magnetic resonance imaging', *Neurocrit Care,* 7 (1), 92-100.

Cheng, A., et al. (1997), 'Three-dimensional organization of a human water channel', *Nature,* 387 (6633), 627-30.

Claassen, J., et al. (2002), 'Global cerebral edema after subarachnoid hemorrhage: frequency, predictors, and impact on outcome', *Stroke,* 33 (5), 1225-32.

Crockard, A., Hayward, R., and Hoff, JT (2000), *Neurosurgery. The Scientific Basis of Clinical Practice*, 2 vols. (Third edn., 1).

Cserr, H. F., et al. (1981), 'Efflux of radiolabeled polyethylene glycols and albumin from rat brain', *Am J Physiol,* 240 (4), F319-28.

Cutler, R. W., et al. (1968), 'Formation and absorption of cerebrospinal fluid in man', *Brain,* 91 (4), 707-20.

Davison, H. and Segal, M.B. (1996), *Physiology of the CSF and Blodd Brain Barriers* (Boca Raton).

de Groot, B. L., et al. (2003), 'The mechanism of proton exclusion in the aquaporin-1 water channel', *J Mol Biol,* 333 (2), 279-93.

de Rooij, N. K., et al. (2007), 'Incidence of subarachnoid haemorrhage: a systematic review with emphasis on region, age, gender and time trends', *J Neurol Neurosurg Psychiatry,* 78 (12), 1365-72.

Del Bigio, M. R. (1995), 'The ependyma: a protective barrier between brain and cerebrospinal fluid', *Glia,* 14 (1), 1-13.

Denker, B. M., et al. (1988), 'Identification, purification, and partial characterization of a novel Mr 28,000 integral membrane protein from erythrocytes and renal tubules', *J Biol Chem,* 263 (30), 15634-42.

Ding, J. H., et al. (2007), 'Alterations of striatal neurotransmitter release in aquaporin-4 deficient mice: An in vivo microdialysis study', *Neurosci Lett,* 422 (3), 175-80.

Dobrogowska, D. H., et al. (1998), 'Increased blood-brain barrier permeability and endothelial abnormalities induced by vascular endothelial growth factor', *J Neurocytol,* 27 (3), 163-73.

Doczi, T., et al. (1982), 'Brain water accumulation after the central administration of vasopressin', *Neurosurgery,* 11 (3), 402-7.

Dolman, D., et al. (2005), 'Induction of aquaporin 1 but not aquaporin 4 messenger RNA in rat primary brain microvessel endothelial cells in culture', *J Neurochem,* 93 (4), 825-33.

Edsbagge, M., et al. (2004), 'Spinal CSF absorption in healthy individuals', *Am J Physiol Regul Integr Comp Physiol,* 287 (6), R1450-5.

Fan, Y., et al. (2008), 'Hypersensitivity of aquaporin 4-deficient mice to 1-methyl-4-phenyl-1,2,3,6-tetrahydropyrindine and astrocytic modulation', *Neurobiol Aging,* 29 (8), 1226-36.

Fan, Y., et al. (2005), 'Sex- and region-specific alterations of basal amino acid and monoamine metabolism in the brain of aquaporin-4 knockout mice', *J Neurosci Res,* 82 (4), 458-64.

Feng, X., et al. (2008), 'Sporadic obstructive hydrocephalus in Aqp4 null mice', *J Neurosci Res.*

Fields, R. D. and Stevens-Graham, B. (2002), 'New insights into neuron-glia communication', *Science,* 298 (5593), 556-62.

Fishman, R. A. (1975), 'Brain edema', *N Engl J Med,* 293 (14), 706-11.

Foldi, M. (1999), 'The brain and the lymphatic system revisited', *Lymphology,* 32 (2), 40-4.

Furman, C. S., et al. (2003), 'Aquaporin-4 square array assembly: opposing actions of M1 and M23 isoforms', *Proc Natl Acad Sci U S A,* 100 (23), 13609-14.

Goldberg, M. and Handler, J. S. (1960), 'Hyponatremia and renal wasting of sodium in patients with malfunction of the central nervous system', *N Engl J Med,* 263, 1037-43.

Goss, J. R., Finch, C. E., and Morgan, D. G. (1991), 'Age-related changes in glial fibrillary acidic protein mRNA in the mouse brain', *Neurobiol Aging,* 12 (2), 165-70.

Greene, K. A., et al. (1995), 'Impact of traumatic subarachnoid hemorrhage on outcome in nonpenetrating head injury. Part I: A proposed computerized tomography grading scale', *J Neurosurg,* 83 (3), 445-52.

Greitz, D., Greitz, T., and Hindmarsh, T. (1997), 'A new view on the CSF-circulation with the potential for pharmacological treatment of childhood hydrocephalus', *Acta Paediatr,* 86 (2), 125-32.

Groger, U., Huber, P., and Reulen, H. J. (1994), 'Formation and resolution of human peritumoral brain edema', *Acta Neurochir Suppl (Wien),* 60, 373-4.

Grote, E. and Hassler, W. (1988), 'The critical first minutes after subarachnoid hemorrhage', *Neurosurgery,* 22 (4), 654-61.

Gullans, S. R. and Verbalis, J. G. (1993), 'Control of brain volume during hyperosmolar and hypoosmolar conditions', *Annu Rev Med,* 44, 289-301.

Hara, M. and Verkman, A. S. (2003), 'Glycerol replacement corrects defective skin hydration, elasticity, and barrier function in aquaporin-3-deficient mice', *Proc Natl Acad Sci U S A,* 100 (12), 7360-5.

Hara, M., Ma, T., and Verkman, A. S. (2002), 'Selectively reduced glycerol in skin of aquaporin-3-deficient mice may account for impaired skin hydration, elasticity, and barrier recovery', *J Biol Chem,* 277 (48), 46616-21.

Hara-Chikuma, M., et al. (2005), 'Progressive adipocyte hypertrophy in aquaporin-7-deficient mice: adipocyte glycerol permeability as a novel regulator of fat accumulation', *J Biol Chem,* 280 (16), 15493-6.

Hasegawa, H., et al. (1994), 'Molecular cloning of a mercurial-insensitive water channel expressed in selected water-transporting tissues', *J Biol Chem,* 269 (8), 5497-500.

Hoffman, H. J. and Duffner, P. K. (1985), 'Extraneural metastases of central nervous system tumors', *Cancer,* 56 (7 Suppl), 1778-82.

Hop, J. W., et al. (1997), 'Case-fatality rates and functional outcome after subarachnoid hemorrhage: a systematic review', *Stroke,* 28 (3), 660-4.

Ito, U., et al. (1979), 'Brain edema during ischemia and after restoration of blood flow. Measurement of water, sodium, potassium content and plasma protein permeability', *Stroke,* 10 (5), 542-7.

Janzer, R. C. and Raff, M. C. (1987), 'Astrocytes induce blood-brain barrier properties in endothelial cells', *Nature,* 325 (6101), 253-7.

Joynt, R. J., Afifi, A., and Harrison, J. (1965), 'Hyponatremia in subarachnoid hemorrhage', *Arch Neurol,* 13 (6), 633-8.

Jung, J. S., et al. (1994), 'Molecular characterization of an aquaporin cDNA from brain: candidate osmoreceptor and regulator of water balance', *Proc Natl Acad Sci U S A,* 91 (26), 13052-6.

Kamii, H., et al. (1999), 'Amelioration of vasospasm after subarachnoid hemorrhage in transgenic mice overexpressing CuZn-superoxide dismutase', *Stroke,* 30 (4), 867-71; discussion 72.

Kassell, N. F., et al. (1990), 'The International Cooperative Study on the Timing of Aneurysm Surgery. Part 1: Overall management results', *J Neurosurg,* 73 (1), 18-36.

Kimelberg, H. K. (1995), 'Current concepts of brain edema. Review of laboratory investigations', *J Neurosurg,* 83 (6), 1051-9.

Klatzo, I. (1987), 'Pathophysiological aspects of brain edema', *Acta Neuropathol,* 72 (3), 236-9.

--- (1994), 'Evolution of brain edema concepts', *Acta Neurochir Suppl (Wien),* 60, 3-6.

Koh, L., Zakharov, A., and Johnston, M. (2005), 'Integration of the subarachnoid space and lymphatics: is it time to embrace a new concept of cerebrospinal fluid absorption?', *Cerebrospinal Fluid Res,* 2, 6.

Kohn, M. I., et al. (1991), 'Analysis of brain and cerebrospinal fluid volumes with MR imaging. Part I. Methods, reliability, and validation', *Radiology,* 178 (1), 115-22.

Kong, H., et al. (2008), 'Requirement of AQP4 for Antidepressive Efficiency of Fluoxetine: Implication in Adult Hippocampal Neurogenesis', *Neuropsychopharmacology*.

Kuroiwa, T., et al. (1985), 'Role of extracellular proteins in the dynamics of vasogenic brain edema', *Acta Neuropathol,* 66 (1), 3-11.

Lagares, A., et al. (2001), 'Prognostic factors on hospital admission after spontaneous subarachnoid haemorrhage', *Acta Neurochir (Wien),* 143 (7), 665-72.

Li, J. and Verkman, A. S. (2001), 'Impaired hearing in mice lacking aquaporin-4 water channels', *J Biol Chem,* 276 (33), 31233-7.

Li, J., Patil, R. V., and Verkman, A. S. (2002), 'Mildly abnormal retinal function in transgenic mice without Muller cell aquaporin-4 water channels', *Invest Ophthalmol Vis Sci,* 43 (2), 573-9.

Li, Z., et al. (2006), 'Aquaporin-4 knockout regulated cocaine-induced behavior and neurochemical changes in mice', *Neurosci Lett,* 403 (3), 294-8.

Lin, C. L., et al. (2003), 'A murine model of subarachnoid hemorrhage-induced cerebral vasospasm', *J Neurosci Methods,* 123 (1), 89-97.

Liu, Y., et al. (2007), 'Subarachnoid hemorrhage in the subacute stage: elevated apparent diffusion coefficient in normal-appearing brain tissue after treatment', *Radiology,* 242 (2), 518-25.

Lo, W. D., Wolny, A., and Boesel, C. (1994), 'Blood-brain barrier permeability in staphylococcal cerebritis and early brain abscess', *J Neurosurg,* 80 (5), 897-905.

Longatti, P., et al. (2006), 'Aquaporin(s) expression in choroid plexus tumours', *Pediatr Neurosurg,* 42 (4), 228-33.

Lu, M., et al. (1996), 'The human AQP4 gene: definition of the locus encoding two water channel polypeptides in brain', *Proc Natl Acad Sci U S A,* 93 (20), 10908-12.

Ma, T., et al. (1996), 'cDNA cloning and gene structure of a novel water channel expressed exclusively in human kidney: evidence for a gene cluster of aquaporins at chromosome locus 12q13', *Genomics,* 35 (3), 543-50.

Ma, T., et al. (1997), 'Generation and phenotype of a transgenic knockout mouse lacking the mercurial-insensitive water channel aquaporin-4', *J Clin Invest,* 100 (5), 957-62.

Manley, G. T., et al. (2000), 'Aquaporin-4 deletion in mice reduces brain edema after acute water intoxication and ischemic stroke', *Nat Med,* 6 (2), 159-63.

Marmarou, A., et al. (1994), 'Brain edema resolution by CSF pathways and brain vasculature in cats', *Am J Physiol,* 267 (2 Pt 2), H514-20.

Matson, D. D. (1965), 'Treatment of Cerebral Swelling', *N Engl J Med,* 272, 626-8.

Meinild, A. K., Klaerke, D. A., and Zeuthen, T. (1998), 'Bidirectional water fluxes and specificity for small hydrophilic molecules in aquaporins 0-5', *J Biol Chem,* 273 (49), 32446-51.

Meng, S., et al. (2004), 'Correspondence of AQP4 expression and hypoxic-ischaemic brain oedema monitored by magnetic resonance imaging in the immature and juvenile rat', *Eur J Neurosci,* 19 (8), 2261-9.

Milhorat, T. H. (1987), 'Acute hydrocephalus after aneurysmal subarachnoid hemorrhage', *Neurosurgery,* 20 (1), 15-20.

Milhorat, T. H., et al. (1971), 'Cerebrospinal fluid production by the choroid plexus and brain', *Science,* 173 (994), 330-2.

Mullen, R. J., Buck, C. R., and Smith, A. M. (1992), 'NeuN, a neuronal specific nuclear protein in vertebrates', *Development,* 116 (1), 201-11.

Murata, K., et al. (2000), 'Structural determinants of water permeation through aquaporin-1', *Nature,* 407 (6804), 599-605.

Nag, S. (2003), 'Pathophysiology of blood-brain barrier breakdown', *Methods Mol Med,* 89, 97-119.

Nag, S., Venugopalan, R., and Stewart, D. J. (2007), 'Increased caveolin-1 expression precedes decreased expression of occludin and claudin-5 during blood-brain barrier breakdown', *Acta Neuropathol,* 114 (5), 459-69.

Nag, S., Manias, J. L., and Stewart, D. J. (2009a), 'Expression of endothelial phosphorylated caveolin-1 is increased in brain injury', *Neuropathol Appl Neurobiol,* 35 (4), 417-26.

--- (2009b), 'Pathology and new players in the pathogenesis of brain edema', *Acta Neuropathol,* 118 (2), 197-217.

Nagelhus, E. A., et al. (1999), 'Immunogold evidence suggests that coupling of K+ siphoning and water transport in rat retinal Muller cells is mediated by a coenrichment of Kir4.1 and AQP4 in specific membrane domains', *Glia,* 26 (1), 47-54.

Neely, J. D., et al. (1999), 'Heterotetrameric composition of aquaporin-4 water channels', *Biochemistry,* 38 (34), 11156-63.

Neely, J. D., et al. (2001), 'Syntrophin-dependent expression and localization of Aquaporin-4 water channel protein', *Proc Natl Acad Sci U S A,* 98 (24), 14108-13.

Nicholson, C., et al. (2000), 'Diffusion of molecules in brain extracellular space: theory and experiment', *Prog Brain Res,* 125, 129-54.

Nielsen, S., et al. (1993), 'Distribution of the aquaporin CHIP in secretory and resorptive epithelia and capillary endothelia', *Proc Natl Acad Sci U S A,* 90 (15), 7275-9.

Nielsen, S., et al. (1997), 'Specialized membrane domains for water transport in glial cells: high-resolution immunogold cytochemistry of aquaporin-4 in rat brain', *J Neurosci,* 17 (1), 171-80.

Ohata, K., Marmarou, A., and Povlishock, J. T. (1990), 'An immunocytochemical study of protein clearance in brain infusion edema', *Acta Neuropathol,* 81 (2), 162-77.

Oshio, K., et al. (2005), 'Reduced cerebrospinal fluid production and intracranial pressure in mice lacking choroid plexus water channel Aquaporin-1', *Faseb J,* 19 (1), 76-8.

Oshio, K., et al. (2006), 'Impaired pain sensation in mice lacking Aquaporin-1 water channels', *Biochem Biophys Res Commun,* 341 (4), 1022-8.

Oshio, K., et al. (2004), 'Expression of aquaporin water channels in mouse spinal cord', *Neuroscience,* 127 (3), 685-93.

Owens, T., Bechmann, I., and Engelhardt, B. (2008), 'Perivascular spaces and the two steps to neuroinflammation', *J Neuropathol Exp Neurol,* 67 (12), 1113-21.

Papadopoulos, M. C. and Verkman, A. S. (2005), 'Aquaporin-4 gene disruption in mice reduces brain swelling and mortality in pneumococcal meningitis', *J Biol Chem,* 280 (14), 13906-12.

Papadopoulos, M. C., Saadoun, S., and Verkman, A. S. (2008), 'Aquaporins and cell migration', *Pflugers Archiv,* In press.

Papadopoulos, M. C., et al. (2004), 'Aquaporin-4 facilitates reabsorption of excess fluid in vasogenic brain edema', ***Faseb J,*** **18 (11), 1291-3.**

Parra, A., et al. (2002), 'Mouse model of subarachnoid hemorrhage associated cerebral vasospasm: methodological analysis', ***Neurol Res,*** **24 (5), 510-6.**

Pobereskin, L. H. (2001), 'Incidence and outcome of subarachnoid haemorrhage: a retrospective population based study', ***J Neurol Neurosurg Psychiatry,*** **70 (3), 340-3.**

Preston, G. M., et al. (1992), 'Appearance of water channels in Xenopus oocytes expressing red cell CHIP28 protein', ***Science,*** **256 (5055), 385-7.**

Prunell, G. F., Mathiesen, T., and Svendgaard, N. A. (2002), 'A new experimental model in rats for study of the pathophysiology of subarachnoid hemorrhage', ***Neuroreport,*** **13 (18), 2553-6.**

Rabinstein, A. A. (2006), 'Treatment of cerebral edema', ***Neurologist,*** **12 (2), 59-73.**

Rash, J. E., et al. (1998), 'Direct immunogold labeling of aquaporin-4 in square arrays of astrocyte and ependymocyte plasma membranes in rat brain and spinal cord', ***Proc Natl Acad Sci U S A,*** **95 (20), 11981-6.**

Reese, T. S. and Karnovsky, M. J. (1967), 'Fine structural localization of a blood-brain barrier to exogenous peroxidase', ***J Cell Biol,*** **34 (1), 207-17.**

Reulen, H. J., et al. (1977), 'Role of pressure gradients and bulk flow in dynamics of vasogenic brain edema', ***J Neurosurg,*** **46 (1), 24-35.**

Reulen, H. J., et al. (1978), 'Clearance of edema fluid into cerebrospinal fluid. A mechanism for resolution of vasogenic brain edema', ***J Neurosurg,*** **48 (5), 754-64.**

Rinkel, G. J., van Gijn, J., and Wijdicks, E. F. (1993), 'Subarachnoid hemorrhage without detectable aneurysm. A review of the causes', *Stroke,* 24 (9), 1403-9.

Rojek, A. M., et al. (2007), 'Defective glycerol metabolism in aquaporin 9 (AQP9) knockout mice', *Proc Natl Acad Sci U S A,* 104 (9), 3609-14.

Saadoun, S., Papadopoulos, M. C., and Krishna, S. (2003), 'Water transport becomes uncoupled from K+ siphoning in brain contusion, bacterial meningitis, and brain tumours: immunohistochemical case review', *J Clin Pathol,* 56 (12), 972-5.

Saadoun, S., et al. (2005a), 'Impairment of angiogenesis and cell migration by targeted aquaporin-1 gene disruption', *Nature,* 434 (7034), 786-92.

Saadoun, S., et al. (2008), 'Greatly improved neurological outcome after spinal cord compression injury in AQP4-deficient mice', *Brain,* 131 (Pt 4), 1087-98.

Saadoun, S., et al. (2002a), 'Aquaporin-4 expression is increased in oedematous human brain tumours', *J Neurol Neurosurg Psychiatry,* 72 (2), 262-5.

Saadoun, S., et al. (2002b), 'Increased aquaporin 1 water channel expression in human brain tumours', *Br J Cancer,* 87 (6), 621-3.

Saadoun, S., et al. (2005b), 'Involvement of aquaporin-4 in astroglial cell migration and glial scar formation', *J Cell Sci,* 118 (Pt 24), 5691-8.

Sage, M. R., Wilson, A. J., and Scroop, R. (1998), 'Contrast media and the brain. The basis of CT and MR imaging enhancement', *Neuroimaging Clin N Am,* 8 (3), 695-707.

Saito, A., et al. (2001), 'Transgenic CuZn-superoxide dismutase inhibits NO synthase induction in experimental subarachnoid hemorrhage', *Stroke,* 32 (7), 1652-7.

Schoonman, G. G., et al. (2008), 'Hypoxia-induced acute mountain sickness is associated with intracellular cerebral edema: a 3 T magnetic resonance imaging study', *J Cereb Blood Flow Metab,* 28 (1), 198-206.

Seitz, R. J. and Wechsler, W. (1987), 'Immunohistochemical demonstration of serum proteins in human cerebral gliomas', *Acta Neuropathol,* 73 (2), 145-52.

Shi, L. B., Skach, W. R., and Verkman, A. S. (1994), 'Functional independence of monomeric CHIP28 water channels revealed by expression of wild-type mutant heterodimers', *J Biol Chem,* 269 (14), 10417-22.

Shields, S. D., et al. (2007), 'Anatomical and functional analysis of aquaporin 1, a water channel in primary afferent neurons', *Pain,* 131 (1-2), 8-20.

Sidel, V. W. and Solomon, A. K. (1957), 'Entrance of water into human red cells under an osmotic pressure gradient', *J Gen Physiol,* 41 (2), 243-57.

Solomon, R. A., et al. (1985), 'Decrease in cerebral blood flow in rats after experimental subarachnoid hemorrhage: a new animal model', *Stroke,* 16 (1), 58-64.

Song, Y. and Verkman, A. S. (2001), 'Aquaporin-5 dependent fluid secretion in airway submucosal glands', *J Biol Chem,* 276 (44), 41288-92.

Song, Y., Sonawane, N., and Verkman, A. S. (2002), 'Localization of aquaporin-5 in sweat glands and functional analysis using knockout mice', *J Physiol,* 541 (Pt 2), 561-8.

Songyang, Z., et al. (1997), 'Recognition of unique carboxyl-terminal motifs by distinct PDZ domains', *Science,* 275 (5296), 73-7.

Sui, H., et al. (2001), 'Structural basis of water-specific transport through the AQP1 water channel', *Nature,* 414 (6866), 872-8.

Sun, M. C., et al. (2003), 'Regulation of aquaporin-4 in a traumatic brain injury model in rats', *J Neurosurg,* 98 (3), 565-9.

Sun, X. L., et al. (2007), 'Aquaporin 4 regulates the effects of ovarian hormones on monoamine neurotransmission', *Biochem Biophys Res Commun,* 353 (2), 457-62.

Sun, X. L., et al. (2008), 'Aquaporin-4 deficiency induces subfertility in female mice', *Fertil Steril.*

Sykova, E. (1997), 'Extracellular space volume and geometry of the rat brain after ischemia and central injury', *Adv Neurol,* 73, 121-35.

Sykova, E. and Nicholson, C. (2008), 'Diffusion in brain extracellular space', *Physiol Rev,* 88 (4), 1277-340.

Tait, M. J., et al. (2008), 'Water movements in the brain: role of aquaporins', *Trends Neurosci,* 31 (1), 37-43.

Tajima, M., Crane, J. M., and Verkman, A. S. (2010), 'Aquaporin-4 (AQP4) associations and array dynamics probed by photobleaching and single-molecule analysis of green fluorescent protein-AQP4 chimeras', *J Biol Chem,* 285 (11), 8163-70.

Tripathi, B. J. and Tripathi, R. C. (1974), 'Vacuolar transcellular channels as a drainage pathway for cerebrospinal fluid', *J Physiol,* 239 (1), 195-206.

Trojanowski, T. (1984), 'Early effects of experimental arterial subarachnoid haemorrhage on the cerebral circulation. Part I: Experimental subarachnoid haemorrhage in cat and its pathophysiological effects. Methods of regional cerebral blood flow measurement and evaluation of microcirculation', *Acta Neurochir (Wien),* 72 (1-2), 79-94.

Tsuyumu, M., Reulen, H. J., and Prioleau, G. (1981), 'Dynamics of formation and resolution of vasogenic brain oedema. I. Measurement of oedema clearance into ventricular CSF', *Acta Neurochir (Wien),* 57 (1-2), 1-13.

Unterberg, A. W., et al. (2004), 'Edema and brain trauma', *Neuroscience,* 129 (4), 1021-9.

Vaquero, J. and Butterworth, R. F. (2007), 'Mechanisms of brain edema in acute liver failure and impact of novel therapeutic interventions', *Neurol Res,* 29 (7), 683-90.

Veelken, J. A., Laing, R. J., and Jakubowski, J. (1995), 'The Sheffield model of subarachnoid hemorrhage in rats', *Stroke,* 26 (7), 1279-83; discussion 84.

Verkman, A. S. (2005), 'More than just water channels: unexpected cellular roles of aquaporins', *J Cell Sci,* 118 (Pt 15), 3225-32.

--- (2006), 'Roles of aquaporins in kidney revealed by transgenic mice', *Semin Nephrol,* 26 (3), 200-8.

Voldby, B. and Enevoldsen, E. M. (1982), 'Intracranial pressure changes following aneurysm rupture. Part 1: clinical and angiographic correlations', *J Neurosurg,* 56 (2), 186-96.

Vorbrodt, A. W. and Dobrogowska, D. H. (2003), 'Molecular anatomy of intercellular junctions in brain endothelial and epithelial barriers: electron microscopist's view', *Brain Res Brain Res Rev,* 42 (3), 221-42.

Walz, T., et al. (1997), 'The three-dimensional structure of aquaporin-1', *Nature,* 387 (6633), 624-7.

Warth, A., et al. (2007), 'Expression pattern of the water channel aquaporin-4 in human gliomas is associated with blood-brain barrier disturbance but not with patient survival', *J Neurosci Res,* 85 (6), 1336-46.

Wasterlain, C. G. and Torack, R. M. (1968), 'Cerebral edema in water intoxication. II. An ultrastructural study', *Arch Neurol,* 19 (1), 79-87.

Wu, N., et al. (2008), 'Aquaporin 4 deficiency modulates morphine pharmacological actions', *Neurosci Lett,* 448 (2), 221-5.

Yang, B. and Verkman, A. S. (1997), 'Water and glycerol permeabilities of aquaporins 1-5 and MIP determined quantitatively by expression of epitope-tagged constructs in Xenopus oocytes', *J Biol Chem,* 272 (26), 16140-6.

Yang, B., van Hoek, A. N., and Verkman, A. S. (1997), 'Very high single channel water permeability of aquaporin-4 in baculovirus-infected insect cells and liposomes reconstituted with purified aquaporin-4', *Biochemistry,* 36 (24), 7625-32.

Yang, B., Zador, Z., and Verkman, A. S. (2008), 'Glial cell aquaporin-4 overexpression in transgenic mice accelerates cytotoxic brain swelling', *J Biol Chem,* 283 (22), 15280-6.

Yang, B., et al. (2000), 'Skeletal muscle function and water permeability in aquaporin-4 deficient mice', *Am J Physiol Cell Physiol,* 278 (6), C1108-15.

Yao, X., et al. (2008), 'Aquaporin-4-deficient mice have increased extracellular space without tortuosity change', *J Neurosci,* 28 (21), 5460-4.

Yeung, D., et al. (2008), 'Decreased junctional adhesion molecule-A expression during blood-brain barrier breakdown', *Acta Neuropathol,* 115 (6), 635-42.

Zador, Z., et al. (2008), 'Microfiberoptic fluorescence photobleaching reveals size-dependent macromolecule diffusion in extracellular space deep in brain', *Faseb J,* 22 (3), 870-9.

Zeng, X. N., et al. (2007), 'Aquaporin-4 deficiency down-regulates glutamate uptake and GLT-1 expression in astrocytes', *Mol Cell Neurosci,* 34 (1), 34-9.

Zhao, J., et al. (2005), 'Sulforaphane enhances aquaporin-4 expression and decreases cerebral edema following traumatic brain injury', *J Neurosci Res,* 82 (4), 499-506.

Zhou, J., et al. (2008), 'Altered blood-brain barrier integrity in adult aquaporin-4 knockout mice', *Neuroreport,* 19 (1), 1-5.